

Equilibria among Fe-Ti oxides, pyroxenes, olivine, and quartz: Part II. Application

B. RONALD FROST

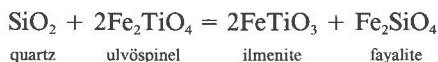
Department of Geology and Geophysics, University of Wyoming, Laramie, Wyoming 82071, U.S.A.

DONALD H. LINDSLEY

Center for High-Pressure Research, Department of Earth and Space Sciences, State University of New York, Stony Brook, New York 11794, U.S.A.

ABSTRACT

Relations among Fe-Ti oxides, calcium magnesium iron pyroxenes and olivines, and quartz are governed by the reaction QUIIF:



and numerous derivative equilibria in the system Fe-O-CaO-MgO-SiO₂-TiO₂. By combining internally consistent thermodynamic solution models for iron magnesium titanium oxides and calcium magnesium iron pyroxenes and olivines, we have calibrated these equilibria (Lindsley and Frost, 1992). In this paper we show how they are applied to the interpretation of a wide range of volcanic and plutonic rocks. Depending on the assemblage, the pyroxene QUIIF equilibria permit calculation of temperature, pressure, f_{O_2} , and silica activity for numerous rocks.

Pyroxene QUIIF equilibria place constraints on the intrinsic parameters that controlled the evolution of three well-studied igneous bodies: the Bishop Tuff, Thingmuli Volcano, and the Skaergaard Intrusion. The Fe-Ti oxides of the Bishop Tuff are not in equilibrium with the coexisting pyroxenes and quartz. Compositions of augite, Opx, and titaniferous magnetite are essentially constant throughout the pyroxene-bearing portion of Bishop Tuff and could have been in equilibrium with quartz at 824 ± 15 °C, 2700 ± 2000 bars, and f_{O_2} 1.39 ± 0.05 log units above that of the FMQ buffer. The compositions of the ilmenites have been modified in response to a thermal event not recorded in the pyroxenes that could have occurred either within the magma chamber immediately before the tuff was ejected or possibly within the tuff after eruption.

Thingmuli Volcano in Iceland contains several rock types that have assemblages suitable for applying pyroxene QUIIF. Rocks that contain pigeonite and augite together with ilmenite and single-phase titaniferous magnetite generally have similar pyroxene and oxide temperatures. Pyroxene-QUIIF relations greatly restrict uncertainties in T and f_{O_2} relative to those for oxide data alone.

Crystallization of Skaergaard magma followed a relatively reducing trend from f_{O_2} near FMQ, where oxides first appear, to nearly 2 log units below FMQ in the Sandwich horizon, values that are all higher than those indicated by measurements of intrinsic f_{O_2} . QUIIF relations show unequivocally that the silicates could not have been in equilibrium with any titaniferous magnetite and ilmenite at the f_{O_2} indicated by the intrinsic measurements.

We have also applied the pyroxene QUIIF equilibria to many other rock suites. Calc-alkalic volcanic rocks that contain low-Ca pyroxenes tend to have equilibrated at the same relative f_{O_2} (about 1–2 log units above FMQ) even though they represent a range of composition from andesite to rhyolite. In contrast, tholeiitic volcanic rocks, as typified by Thingmuli, crystallized at much lower f_{O_2} (generally about 1 log unit below FMQ) and, like calc-alkalic suites, show little or no change in relative f_{O_2} with temperature. Plutonic suites show similar ranges in f_{O_2} , with layered gabbros of calc-alkalic affinity having f_{O_2} above that of FMQ and those of tholeiitic affinity having f_{O_2} below FMQ.

INTRODUCTION

Possible phases in the system Fe-O-CaO-MgO-SiO₂-TiO₂ include three pyroxenes (augite, pigeonite, Opx), ol-

ivine, quartz, and two oxides (titaniferous magnetite and ilmenite) (Table 1). Lindsley and Frost (1992) show how these phases and the 59 calibrated equilibria among them can be used to calculate temperature, pressure, f_{O_2} , and

a_{SiO_2} (for quartz-absent assemblages) for a variety of assemblages in many kinds of igneous rocks. In this paper we apply these calcium pyroxene QUIIF equilibria to a variety of volcanic and intrusive rocks. The discussion assumes that the reader is familiar with the background presented in Lindsley and Frost (1992). We use QUIIF (lower case "i") to refer to the method, and QUILF (upper case "L") to refer to the actual program used in calculating the equilibria. We use the term "reset" to refer to any process, such as exsolution or cation exchange, that changes the composition of a primary phase.

ASSUMPTIONS AND REQUIRED INFORMATION FOR APPLYING PYROXENE QUIIF

To apply pyroxene QUIIF or any other thermodynamic model, one must make a number of assumptions: (1) that the minerals of the assemblage were once in equilibrium at a fixed (or limited range of) temperature and pressure, (2) that the minerals have retained their equilibrium compositions or that those compositions can be reconstructed, (3) that the mineral compositions are accurately known, (4) that the effects of components not included in the solution models can be accounted for, and (5) that the thermodynamic model itself is valid.

Assumption 1: The assemblage was in equilibrium

Unfortunately, it is generally easier to demonstrate a lack of equilibrium than its existence. Resorption of a phase, strong (and especially discontinuous) zoning, and reaction textures may all suggest lack of equilibrium. Exsolution (including oxyexsolution in titaniferous magnetite) is proof of resetting, but in favorable cases the petrologist can reconstruct the original phase composition (Buddington and Lindsley, 1964; Bohlen and Essene, 1977). Textural evidence that all phases of interest crystallized simultaneously is permissive evidence for equilibrium. In the long run, it is the skill and experience of the petrographer that are most important.

Assumption 2: The minerals have retained their compositions

Again, the best evidence for this assumption is often a lack of contrary indications. Some cases of resetting, such as exsolution, are obvious. Others may require careful microprobe analyses; if mineral pairs that are adjacent to each other have compositions indicating lower temperatures than pairs that are distant from each other, it is likely that local exchange has occurred. Some resetting seems to be almost inevitable, and it may be necessary to devise ways of getting around it. Lindsley and Frost (1992) and this paper show ways to use pyroxene QUIIF equilibria to test and in some cases to correct for resetting of mineral compositions.

Assumption 3: The mineral compositions are accurately known

All methods of chemical analysis have inherent uncertainties. It is generally accepted that reasonably careful

TABLE 1. Mineral abbreviations, and compositional variables

Abbreviation	Mineral
A, Aug	augite
Cum	cummingtonite
F, Fay	fayalite
H, Hem	hematite
O, Ol	olivine
Op, Opx	orthopyroxene
P, Pig	pigeonite
Q, Qtz	quartz
Il, Ilm	ilmenite
M, Mt	magnetite
TiMt	titaniferous magnetite (magnetite-ulvöspinel solid solution)
U	ulvöspinel (replaces TiMt in QUIIF acronyms)
Variable	Definition
N_{Ti}	number of Ti atoms in titaniferous magnetite (three cations/ four O atoms)
N_{Mg}	number of Mg atoms in titaniferous magnetite (three cations/ four O atoms)
$X_{\text{Fe}}^{\text{Ilm}}$	$\text{MgTiO}_3/(\text{Fe}_2\text{O}_3 + \text{FeTiO}_3 + \text{MgTiO}_3)$ in ilmenite
$X_{\text{Hem}}^{\text{Ilm}}$	$\text{Fe}_2\text{O}_3/(\text{Fe}_2\text{O}_3 + \text{FeTiO}_3 + \text{MgTiO}_3)$ in ilmenite
$X_{\text{Ca}}^{\text{Ol}}$	$\text{Ca}/(\text{Mg} + \text{Fe} + \text{Ca})$ in olivine
$X_{\text{En}}^{\text{Aug}}$	$\text{En}/(\text{En} + \text{Fs} + \text{Wo})$ in augite
$X_{\text{Wo}}^{\text{Aug}}$	$\text{Wo}/(\text{En} + \text{Fs} + \text{Wo})$ in augite
$X_{\text{En}}^{\text{Pig}}$	$\text{En}/(\text{En} + \text{Fs} + \text{Wo})$ in pigeonite
$X_{\text{Wo}}^{\text{Pig}}$	$\text{Wo}/(\text{En} + \text{Fs} + \text{Wo})$ in pigeonite
$X_{\text{En}}^{\text{Opx}}$	$\text{En}/(\text{En} + \text{Fs} + \text{Wo})$ in orthopyroxene
$X_{\text{Wo}}^{\text{Opx}}$	$\text{Wo}/(\text{En} + \text{Fs} + \text{Wo})$ in orthopyroxene

microprobe analysis can usually produce values with an error of approximately 1% (relative) for major elements. If the concentration of the element is low or if the composition of the unknown is very different from that of the standard, the error is likely to be worse. Furthermore, counting statistics alone are likely to result in random errors of 1% (relative). Thus even for competent work, any given individual analysis may have errors approaching 2% (relative). Some common problems are detailed below.

Mg in oxides. Silicate standards generally give unsatisfactory results for oxides. If at all possible, petrologists should use an oxide rather than a silicate standard for Mg during microprobe analyses of magnetite and ilmenite.

Fe³⁺ in ilmenite. Fe³⁺ is not determined directly during microprobe analysis; it must be calculated, usually on the basis of mineral formula. Fe³⁺ in oxide minerals is derived from the difference between Ti and Fe plus other divalent cations, so that the error in Fe³⁺ is essentially the sum of the errors in Fe and Ti. The problem is acute for ilmenite in which the hematite component may be 1 mol% or less. We urge the use of a working standard; the results from any microprobe session should not be accepted unless the ferric content of the working standard can be reproduced.

Fe³⁺ in pyroxene. The ferric content of pyroxenes is generally calculated from charge-balance constraints. Correct assessment of Fe³⁺ is mainly of indirect importance for QUIIF because it affects the apparent Fe²⁺/Mg in the pyroxene. Simply because SiO₂ makes up ~50%

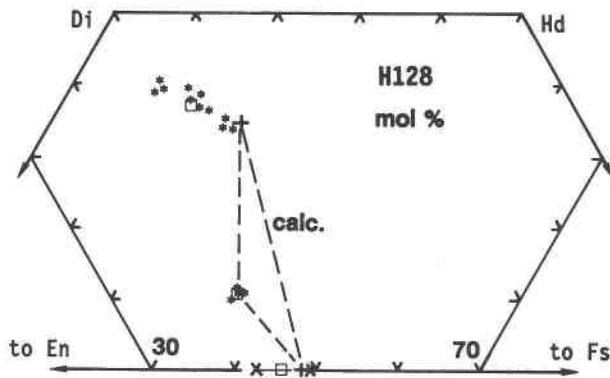


Fig. 1. Portion of the pyroxene quadrilateral showing the published average analyses (squares) of augite, pigeonite, and olivine for sample H128 from Thingmuli (Carmichael, 1967a), projected using PXPROJ. The average analyses do not define an equilibrium assemblage. Also shown are the analyses available only as plotted compositions, projected by Carmichael (asterisks, augite and pigeonite; X--X, olivine). The plus symbols show the augite and olivine that we calculate to have been in equilibrium (dashed tie lines) with the average pigeonite at 1050 °C and 1 bar.

of a typical pyroxene, errors in silica are the most likely cause of error in Fe^{3+} . We suggest that when calculated Fe^{3+} makes up more than approximately 10% of total Fe, the analyst should verify that the composition of a known pyroxene can be reproduced reliably.

Ca in olivine. Accurate analysis of Ca in olivine is important when applying some pyroxene QUIIF equilibria. For example, a_{SiO_2} calculated from the assemblage augite + olivine is critically dependent on the Ca content of the olivine. Ideally, one should use an olivine working standard for Ca, but such standards are rare.

The curse of representative analyses. The common practice of selecting, from a suite of analyses of minerals, one or two for publication as representative is a serious problem for workers who wish to apply thermodynamics to rocks using analyses from the literature. Many published representative phases appear to be far from equilibrium. Yet if we check plots of the analyses, we find that the "representative" analyses may not be representative at all, and that within the scatter of points there are other analyses that could represent equilibrium values. In numerous cases we use those values, but the problem with picking analyses off plots is that we cannot project them rigorously.

Figure 1 illustrates a possible way around the problem of published analyses that do not define an equilibrium pair. Individual augite and pigeonite analyses are shown as published, but only as plotted points. Also shown are the composition of the average pigeonite and the compositions of the augite and olivine calculated to be in equilibrium with it. Those calculated values fall close to the Fe-rich ends of the plotted compositions, in agreement with the petrographic observation that pigeonite occurs only as late-stage overgrowths on augite.

Assumption 4: The effects of other components are addressed

Rocks are complex chemical systems, and it is rare indeed to find an assemblage of minerals that fall precisely into our system $\text{Fe-O-CaO-MgO-SiO}_2\text{-TiO}_2$; other components must be accounted for. Thus projection from real compositional space to the idealized system is necessary. Any projection scheme aims to yield mole fractions that yield the most nearly correct values of activities. We believe that the projection schemes we use generally do this well, but obviously they cannot be perfect.

Assumption 5: The thermodynamic model is valid

It is difficult to detect problems with the solution models used in pyroxene QUIIF. Almost by definition the models are compatible with the experimental data used to construct them, so their ability to reproduce experimental results, although essential, is not a true test. Compatibility with reversed experiments not used in the modeling is clearly a better criterion, and we plan to perform experiments that fall outside the ranges of calibration as a check on the system. However, the ultimate test must be how well the model provides credible and useful data for rocks. This paper is a first step in that testing process.

GOALS AND METHODS

Our goal in this paper is twofold: (1) to illustrate the application of pyroxene QUIIF to a variety of rocks and assemblages and (2) to summarize the data for a number of suites of volcanic and plutonic rocks. The detailed examples are those for which we were able to obtain compositions of all the coexisting phases and had some faith that the minerals represent (or once represented) an equilibrium assemblage. In a review such as this, it is impossible to assess the petrographic controls on all the samples, and thus some of our conclusions may well need revision if the samples are restudied. It is our hope that the examples given here will alert petrologists to the opportunities and requirements of the pyroxene-QUIIF approach as they are studying a suite of rocks.

All mineral analyses used in the calculations discussed in the following sections were projected using our programs OXPROJ and PXPROJ, and thus the values of components we use may vary slightly from most of the values in the original papers. Because the solution models used in program QUIIF specifically account for Mg in the oxides, we have defined the compositional parameters for titaniferous magnetite (Table 1) differently from previous papers. N_{Ti} (equivalent to X_3 of Andersen et al., 1991) is defined as the mole fraction of $\text{Fe}_2\text{TiO}_4 + \text{Mg}_2\text{TiO}_4$ in the titaniferous magnetite. The standard state for a_{SiO_2} is quartz at the indicated pressure and temperature. All f_{O_2} is relative to that of the FMQ buffer: statements regarding f_{O_2} change with temperature are with

respect to values of FMQ, not with respect to absolute values. Igneous rocks form over an interval of temperatures, of course; thus thermometry yields a snapshot that we take to fall within that interval. For the many assemblages involving olivine, pyroxenes, Fe-Ti oxides, and quartz, we use the abbreviations in Table 4 of Lindsley and Frost (1992).

Error analysis

Temperature and f_{O_2} . To illustrate the effects of compositional uncertainty on pyroxene-QUIIF equilibria, we assume an arbitrary assemblage of Opx ($Wo_{3.5}En_{55}Fs_{41.5}$) + augite ($Wo_{37.5}En_{38.8}Fs_{23.7}$) + magnetite ($N_{Ti} = 0.53$, $N_{Mg} = 0.132$) + ilmenite ($Ilm_{74.5}Hem_{13.7}Gk_{11.8}$), which is in equilibrium at 987 °C, 1 kbar, and $\Delta \log f_{O_2}$ (FMQ) = +0.59. We then allow the QUIIF program to calculate temperature and $\Delta \log f_{O_2}$ at 1 and 5 kbar as N_{Ti} and X_{Em}^{Opx} vary by ± 0.01 mole fraction and X_{Wo}^{Opx} vary by 0.002 mole fraction. These uncertainties are realistic for moderately good microprobe analyses. Results are displayed in Figure 2. The effect of pressure is small on temperature and negligible on f_{O_2} ; the pressure effect on $\Delta \log f_{O_2}$ is almost entirely that on the reference FMQ buffer. We chose the initial compositions to lie below quartz saturation (QUIIOpA assemblage; see Lindsley and Frost, 1992) but above olivine saturation (OpAUIIO). The temperatures lie a few tens of degrees below those of pigeonite stability. Had the calculated conditions extended past any of those limits, the stippled polygons in Figure 2 would have been truncated by them (see Lindsley and Frost, 1992, their Figs. 6, 7 for examples of this truncation).

Pressure. In the pyroxene QUIIF system, pressure is best constrained by the equilibrium $Fe_2SiO_4 + SiO_2 = Fe_2Si_2O_6$ (assemblage QOOp). However, assemblages such as quartz + Opx + augite + titaniferous magnetite (QUOpA) or Opx + augite + titaniferous magnetite + olivine (OpAUO) substitute for QOOp and also constrain pressure moderately well. An error of 0.007 mole fraction in X_{Em}^{Opx} (which is close to the expected analytical uncertainty) or of 0.017 mole fraction in N_{Ti} , shifts the pressure estimate by 1000 bars. Thus in favorable cases assemblages like QUOpA and OpAUO can provide pressure estimates to within ± 1500 bars for single analyses of the phases. Using careful multiple analyses can cut that uncertainty in half, provided of course that the phases in the rock are homogeneous.

VOLCANIC SUITES

The Bishop Tuff: An example of the power of the QUIIF approach

The Bishop Tuff (Hildreth, 1977, 1979) is a classic example of a zoned magma body. Hildreth (1979) found a consistent decrease in the temperatures of the Fe-Ti oxides with increasing stratigraphic depth. He interpreted these temperatures as representing a temperature range within the magma chamber such that the first magma erupted was somewhat cooler than magma erupted later.

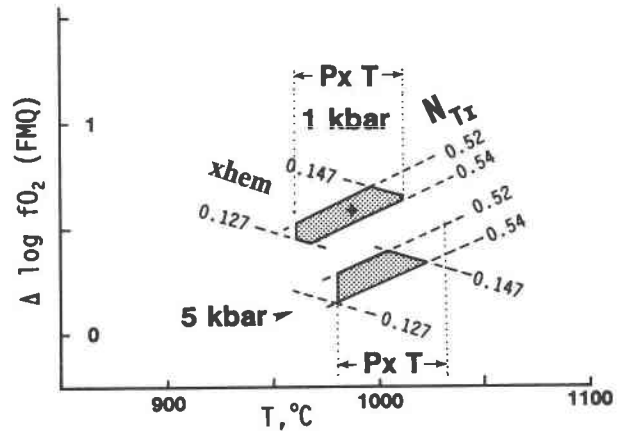


Fig. 2. A diagram of $\Delta \log f_{O_2}$ (FMQ) vs. T showing the effects of errors in composition on conditions calculated using two-pyroxene + two-oxide equilibria. The initial composition (see text) was in equilibrium at 1000 bars, 987 °C, and 0.59 log units above FMQ. The shaded areas show conditions allowed by compositional uncertainties of ± 0.002 in X_{Wo}^{Opx} and ± 0.01 mole fraction in other compositions, for assumed pressures of 1 and 5 kbar. Vertical lines represent the temperature limits allowed by the pyroxene compositions; sloping lines are the limiting isopleths for titaniferous magnetite (N_{Ti}) and ilmenite (X_{hem}).

Recent advances in thermodynamic modeling of oxides with Opx and quartz (Lindsley et al., 1990; Ghiorso and Sack, 1991) permitted us to examine Hildreth's interpretation more closely, for the upper part of the Bishop Tuff contains Opx and augite in addition to the two oxides. Although they used quite different solution models, both Ghiorso and Sack (1991) and Lindsley et al. (1990) found that Opx in the Bishop Tuff was not in equilibrium with the two Fe-Ti oxides and quartz.

The calcium pyroxene QUIIF system permits us to evaluate the pyroxene-bearing portions of the Bishop Tuff even more rigorously. Hildreth (1977) gave analyses of 22 augite-Opx pairs for which the coexisting oxides pass the Mg/Mn equilibrium test of Bacon and Hirschmann (1988). The pyroxene compositions show little variation, and the augite and Opx are in equilibrium according to our solution model. The average temperature for these pyroxene pairs is 824 °C, with a precision (2σ) of ± 15 °C; we estimate the accuracy at approximately ± 30 °C. The oxides from the same 22 samples give temperatures ranging from 764 to 811 °C. Thus, for only a few of these samples are the oxide and pyroxene temperatures compatible. The range in oxide temperatures results entirely from varying Fe_2O_3 contents of the ilmenite; the magnetite clusters tightly around a composition of $N_{Ti} = 0.26$. For this reason, and because most of the oxides have Mg contents too low to have been in equilibrium with the pyroxenes, Frost and Lindsley (1991) and Lindsley et al. (1991) concluded that the oxides must have reequilibrated after eruption of the Bishop Tuff. That conclusion was controversial and disturbing, since if oxides could reset in a (relatively) quickly cooled eruptive sequence, it is

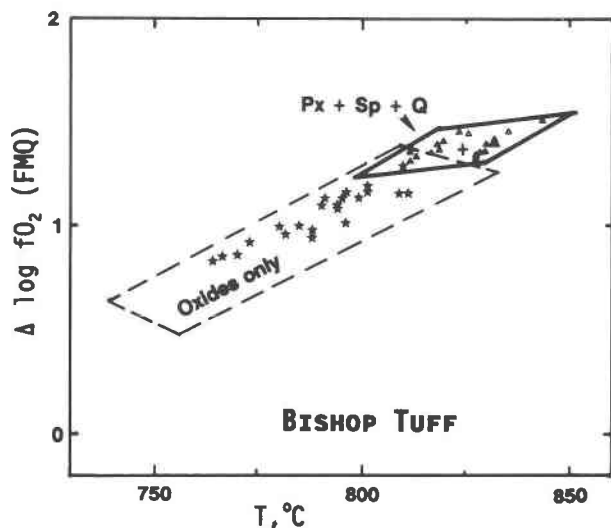


Fig. 3. A diagram of $\Delta \log f_{O_2}$ (FMQ) vs. T calculated for Px-bearing portions of the Bishop Tuff. The f_{O_2} for pyroxene pairs (triangles) was calculated for the Opx + augite + titaniferous magnetite ($N_{Ti} = 0.26$) + quartz assemblage. Individual points are calculated for the published compositions (Hildreth, 1977), projected using our programs PXPJOJ and OXPJOJWT. The plus sign shows conditions for the average pyroxene pair, which has the composition $Wo_{2.05 \pm 0.05}En_{52.7 \pm 0.71}$ (Opx) and $Wo_{4.20 \pm 0.39}En_{38.7 \pm 0.88}$ (Aug). The stars show T and $\Delta \log f_{O_2}$ for oxides only, and the dashed lines show the envelope of uncertainty for the oxides assuming errors of ± 0.005 for N_{Ti} . The solid polygon outlines the conditions based on twice the standard deviations for the pyroxenes. The results show that most oxides are out of equilibrium with the pyroxenes and quartz.

hard to imagine natural conditions in which they would not reset.

An alternative explanation is suggested by the recent work of Lu and Anderson (1991; Lu, personal communication, 1991). They argue that the Bishop Tuff reflects two different magmas that only partially mixed before eruption: (1) a lower temperature, Px-free magma that was low in Mg, Fe, and Mn, and (2) a higher temperature, Px-bearing magma that had higher contents of Mg, Fe, and Mn. We do not review all their arguments here, but one observation is critical. Some Px-bearing samples contain two populations of titaniferous magnetites (both with N_{Ti} of 0.26): low-Mg titaniferous magnetite as inclusions in quartz and higher-Mg titaniferous magnetite as individual grains within the glass. The latter grains approach Fe-Mg exchange equilibrium with the pyroxenes. Lu and Anderson interpret these samples to reflect magma mixing: early, low-Mg titaniferous magnetite enclosed in quartz was protected from reequilibration when its parental magma mixed with a hotter, more Mg-rich, Px-bearing magma. For the present purposes, it is not necessary that chemical mixing be thorough. All that is needed is that a thermal gradient would have been established within the hybrid magma chamber over a period long enough for the oxide, but not the pyroxene, temper-

atures to reset. There are two reasons that it is ilmenite rather than the titaniferous magnetite that shows varying composition. First, the modal abundance of titaniferous magnetite is much greater than that of ilmenite and, second, the Ti contents of titaniferous magnetite in both magmas were fortuitously the same; thus, if the magmas were originally of different temperatures, the ilmenites must have had different compositions. The Lu-Anderson interpretation, like that of Hildreth (1977), suggests a magma chamber zoned from hotter at the bottom to cooler at the top; the main difference lies in how the thermal zoning came about.

Regardless of when the temperature range shown by the oxides was formed, we can use pyroxene-QUIIF equilibria to constrain preeruption conditions within the magma chamber. Because quartz is present, and augite, Opx, and titaniferous magnetite all have tightly constrained compositions, we can calculate the conditions at which those phases and an ilmenite would have been in equilibrium. For the 22 samples mentioned above, the compositions of titaniferous magnetite, augite, and Opx cluster so tightly that it is reasonable to assume the phases are uniform and that the variations result from random error. Thus we have used average compositions and have calculated conditions assuming 2 sd for the average values. The calculated pressure of equilibration is 2758 bars, based on the average compositions, with a 2 σ range from 517 to 4868 bars. Pressures calculated for individual samples range from 2100 to 3300 bars. Figure 3 is a diagram of T vs. $\Delta \log f_{O_2}$ for Px-bearing samples of Bishop Tuff. The points are for the analyses as published, with f_{O_2} for the pyroxenes calculated for the assemblage of Opx + augite + TiMt + quartz. The solid polygon outlines the possible range in T and $\Delta \log f_{O_2}$ allowed by 2 σ deviations for the average compositions of titaniferous magnetite and pyroxenes, and the dashed outline shows the uncertainty based on estimated errors for the oxide analyses.

There are two important features to be deduced from Figure 3. The first is that, in the pyroxene-bearing portions of the Bishop Tuff, the majority of oxides were not in mutual equilibrium with the pyroxenes + quartz; clearly it is the ilmenite composition that is aberrant. The most logical conclusion is that the ilmenite changed composition during a cooling event that was short enough to preclude detectable resetting of the pyroxenes. The second point is that one may use the augite + Opx + TiMt + quartz assemblage to constrain the conditions at which the phases had been in equilibrium.

Thingmuli

The lavas of Thingmuli, a Tertiary volcano in Iceland, have a number of assemblages suitable for illustrating the power of pyroxene QUIIF. The rocks range from olivine tholeiite, through basaltic andesite and icelandite, to rhyolite (Carmichael, 1967a, 1967b). All contain two oxides and augite; most also contain pigeonite, and approximately one-half also have olivine. The data set is also

unusual in having groundmass mineral analyses. Furthermore, in approximately one-half of the samples, the titaniferous magnetite phase has clearly reset by oxidation-exsolution (the "unmixed" spinels of Carmichael, 1967b), whereas the remaining titaniferous magnetite appears primary. Thus these samples provide a welcome opportunity to test the ability of the pyroxene QUIIF equilibria to establish primary compositions prior to the resetting of the titaniferous magnetite compositions. It is intriguing that all the reset titaniferous magnetite samples, which presumably were oxidized at subsolidus temperatures, are distinctly out of Fe-Mg exchange equilibrium with the ferromagnesian silicates, whereas most of the single-phase titaniferous magnetite and the ilmenites are at or close to Fe-Mg exchange equilibrium, with the silicates at the inferred magmatic temperatures. We take these observations to mean (1) that high-temperature Fe-Mg equilibrium can be retained, (2) that the equilibrium can be reset to lower temperatures relatively easily, and (3) that our thermodynamic models are in reasonable agreement with natural assemblages.

In all cases where the oxides do appear to be in exchange equilibrium with the silicates, it is with silicates that are the most Fe rich. We interpret this to mean that the Fe-Mg exchange continues down to the solidus (Roeder and Campbell, 1985, reached a similar conclusion regarding chromite and ferromagnesian silicates). As a result, even though some of the oxides are microphenocrysts and thus may have formed prior to or during eruption, we assume that they equilibrated with the groundmass phases. In view of that, when applying the pyroxene QUIIF equilibria, we used the compositions of the most Fe-rich silicates.

One difficulty in working with the Thingmuli samples is that the pyroxene and olivine analyses are averages of zoned material, and there is no a priori reason to believe that the average compositions would represent equilibrium assemblages. Fortunately, the individual analyses are presented as quadrilateral plots, and it is possible to obtain the Wo-En-Fs and Fo-Fay values from these. We solved the problem of projection as follows: We projected the average analyses using PXP PROJ and compared our projected values of Wo, En, and Fs with those reported by Carmichael (1967a). We then used the deviations between the results of the two projections to correct the plotted points for use in pyroxene QUIIF.

Tholeiites. Carmichael (1967a) reported three tholeiites (G84, G99, G244) that contain single-phase TiMt (N_{Ti} near 0.8) + ilmenite (X_{Hem} near 0.05–0.06) + pigeonite + augite. Within analytical error, these assemblages can have been in equilibrium at 1077–1119 °C, with $\Delta \log f_{O_2}$ approximately 1 log unit below FMQ (Fig. 4, area A; Table 2). Because the pyroxenes are groundmass phases, we used 1 bar in the final calculations. Carmichael (1967a, his Table 2) inferred similar temperatures, but the uncertainties for the oxides alone are much larger (± 115 °C) than for the oxide + pyroxene assemblage.

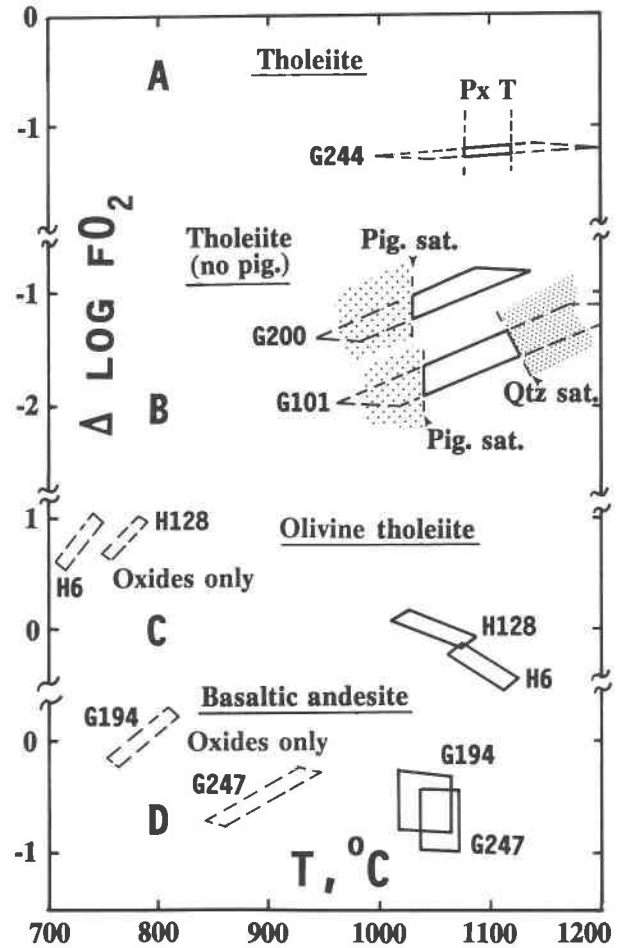


Fig. 4. A diagram of $\Delta \log f_{O_2}$ (FMQ) vs. T inferred conditions for Thingmuli (Carmichael, 1967a). A = tholeiite G244, which has two oxides plus pigeonite and augite. Pyroxene temperatures greatly limit the range permitted by the oxides (parallelogram). Tholeiites G84 and G99 would probably be similar, but the available pyroxene compositions do not permit such tight limits. B = tholeiites G101 and G200, which have augite but no pigeonite reported. The vertical lines labeled Pig. sat. show the temperatures at which the augite would have been in equilibrium with pigeonite; they thus provide minimum temperatures for the assemblage. C = olivine tholeiites H6 and H128, for which the titaniferous magnetite is reported to have reset (unmixed). Temperatures based on the reported oxide compositions clearly represent subsolidus oxidation; calculation of the conditions at which the olivine, augite, and ilmenite for these samples could have been in equilibrium with a more Ti-rich magnetite yields the conditions shown by the solid parallelograms. D = basaltic andesites G194 and G247, which also contain reset titaniferous magnetites. The solid figures show the conditions at which the reported pigeonite, augite, and ilmenite can have been in equilibrium with a more Ti-rich magnetite. The vertical lines show pyroxene temperatures; subhorizontal limits are ilmenite isopleths, allowing for ± 0.01 uncertainty in X_{Hem} . Sample H20 would have overlapped the conditions for G194 and has been omitted for clarity.

TABLE 2. List of volcanic suites

Sample no.	Rock type	Assemblage	P (bar) ^a	T (°C)	Max f_{O_2}	Min f_{O_2}	Re- marks	Ref
Bishop (California)								
	rhyolite	Opx + Aug + Q + TiMt + Ilm	2700 ± 600	824 ± 10	1.43	1.34	see text	1
Cold Bay (Alaska)								
37	andesite	Ol + Opx + Aug + TiMt	(1000–5000)	980–1050 ^b	1.0 ^c	0.6 ^c		2, 3
51	dacite	Opx + Aug + TiMt	(1000–5000)	902–950 ^b	1.9–2.0 ^d	0.75–0.9 ^e		
66	andesite	Opx + Aug + TiMt + Ilm	(1000–5000)	943–968	1.52–1.65	1.1–1.2	e	
80	andesite	Ol + Opx + Aug + TiMt	(1000–5000)	940–1020 ^b	1.3 ^c	1.8 ^c		
Crater Lake (Oregon)								
227	rhyodacite	Opx + Aug + TiMt + Ilm	(1000–5000)	848–868	1.3–1.4	0.8–0.9	e	4
566	rhyodacite	Opx + Aug + TiMt + Ilm	(1000–5000)	900–975 ^b	2.2–2.5 ^f	0.9 ^g		
846	rhyodacite	Opx + Aug + TiMt + Ilm	(1000–5000)	877–892	1.6–1.5	1.1–1.2	e	
871	scoria	Opx + Aug + TiMt + Ilm	(1000–5000)	960–1008	1.4–1.65	1.1–1.3	e	
Erta Ale and Boina (Ethiopia)								
D214	trachyte	Ol + Aug + TiMt + Ilm	(1000–5000)	1060–1140	0.0 to –0.1 ^h	–0.3 to –0.4 ^h	i	5
Erta Ale								
D217	alkali	Ol + Aug + TiMt + Ilm	(1000–5000)	690–760	–0.85 to –1.3 ^h	–1.2 to –1.65 ^h	e	
Erta Ale	rhyolite							
D232	rhyolitic	Ol + Aug + TiMt + Ilm	1	870–890	–0.25 to –0.3 ^h	–0.40 ^h	i	
Erta Ale	trachyte							
TD25	trachyte	Ol + Aug + Ilm + TiMt	1	1020–1055	0 ^h	–0.12 ^h	i	
Boina								
Katmai (Alaska)								
K42	rhyolite	Opx + Q + TiMt + Ilm	4430 ± 800	821–852	1.00 ⁱ	0.95 ⁱ	k	6
K45	dacite	Opx + Aug + TiMt + Ilm	(2000–5000) ^j	853–966 ^b	1.4–1.9 ⁱ	1.0–1.3 ^m		
K101	dacite	Opx + Aug + TiMt + Ilm	(2000–5000) ^j	918–970 ^b	1.6–1.7 ⁱ	1.0 ^m		
K139	rhyolite	Opx + Q + TiMt + Ilm	2900 ± 800	820–844	1.14 ⁱ	1.08 ⁱ	k	
Haroharo (New Zealand)								
A1	rhyolite	Opx + Q + TiMt + Ilm	<500	796–802	1.72 ⁱ	1.54 ⁱ	k	7
A4	rhyolite	Opx + Cum + Q + TiMt + Ilm	1–1860	770–802	1.37 ⁱ	1.27 ⁱ	k	
Okataina (New Zealand)								
A5	rhyolite	Opx + Cum + Q + TiMt + Ilm	1–1408	768–795	1.49 ⁱ	1.40 ⁱ	k	8
A6	dacite	Opx + Aug + TiMt + Ilm	(1000–2000)	930–990 ^b	1.5–1.7 ⁱ	1.2–1.4 ^m		
A6a	dacite	Opx + Aug + TiMt + Ilm	(1000–2000)	960–1000 ^b	1.5–1.7 ⁱ	1.0–1.1 ^m		
A7	rhyolite	Opx + Q + TiMt + Ilm	800–2700	760–798	1.586 ⁱ	1.478 ⁱ	k	
Taupo (New Zealand)								
A10	rhyolite	Opx + Aug + Fay + Q + TiMt + Ilm	1300–1800	850–870	0.59	0.59	n	9
27833	rhyolite	Opx + Q + TiMt + Ilm	(1000–2000)	850–880	0.50 ⁱ	0.47 ⁱ	k	

Two other tholeiites (G101, G200) lack pigeonite, and thus one cannot test whether the oxides give the same temperatures as do pyroxene pairs. Nevertheless, QUIIF equilibria still permit us to place limits on the large temperature uncertainty resulting from the oxides alone (Fig. 4, area B). The minimum temperature for G101 is 1040 °C, or else pigeonite would have joined the assemblage; the maximum temperature (1130 °C) represents quartz saturation.

The two olivine tholeiites (H6, H128) both contain reset titaniferous magnetite. Thus we allow the QUIIF program to calculate a titaniferous magnetite sample that would be in equilibrium with the ilmenite, augite, pigeonite, and olivine (Fig. 4, area C). The temperature range (1062–1125 °C) and calculated titaniferous magnetite for H6 are similar to those for tholeiites with single-phase titaniferous magnetite; thus we are encouraged that the recalculation gives a reasonable approximation to the original titaniferous magnetite composition. Temperatures inferred from pyroxene QUIIF equilibria are distinctly higher than those reported by Carmichael (1967a) from the oxides alone (700–775 °C).

Basaltic andesites. The basaltic andesites (G194, G247, H20) contain ilmenite, pigeonite, augite, and reset titaniferous magnetite; the oxide temperatures are 840, 975, and 850 °C (Carmichael, 1967a, his Table 2). By calculating the titaniferous magnetite that would have been in equilibrium with the other phases, we infer much higher temperatures (1013–1074 °C) and titaniferous magnetite compositions close to those of single-phase titaniferous magnetite from the tholeiites (Table 2; Fig. 4, area D).

Icelandites. Two icelandites were reported by Carmichael (1967a), but only H96A appears to have augite and olivine in equilibrium. Because these are phenocrysts, we calculated conditions for 1, 500, and 1000 bars; the best fit was for 500 bars, although that should not be considered a rigorously constrained pressure. The olivine and augite could have been in equilibrium with the reported ilmenite and a recalculated titaniferous magnetite at 878–967 °C, somewhat higher than the 810 °C estimated using ilmenite and the reset titaniferous magnetite alone. The assemblage is essentially at quartz saturation.

Calculated silica activities for Thingmuli lavas range from 0.82 to 0.84 in the olivine tholeiites, through 0.85–

TABLE 2.—Continued

Sample no.	Rock type	Assemblage	P (bar) ^a	T (°C)	Max f_{O_2}	Min f_{O_2}	Re- marks	Ref
Seguam (Alaska)								
B87-9	basaltic andesite	Ol + Opx + Aug + TiMt + Ilm	(1000–5000)	1080–1150 ^{b,o}	2.4 ⁱ	1.1 ^m	p	10
B87-52	dacite	Opx + Aug + TiMt	(1000–5000)	1030–1095 ^b	1.7–1.9 ^a	1.0–1.2 ^c		
B87-56	dacite	Opx + Aug + TiMt	(1000–5000)	1010–1035 ^b	0.9–1.2 ^d	0.3–0.4 ^c		
Thingmuli (Iceland)								
G151	rhyolite	Fay + Aug + Q + TiMt + Ilm	<3 kbar	860–900	–0.4	–0.7	e, r	11
G194	basaltic andesite	Aug + Pig + TiMt + Ilm	(1)	1017–1065	–0.3	–0.8	e	
G244	tholeiite	Aug + Pig + TiMt + Ilm	(1)	1077–1119	0.74	1.16	e	
G247	tholeiite	Aug + Pig + TiMt + Ilm	(1)	1033–1074 ^b	–0.4 ^s	–1.0 ^s		
H6	basaltic andesite	Ol + Aug + Pig + TiMt + Ilm	1	1062–1125	–0.18	–0.58	e	
H20	basaltic andesite	Aug + Pig + TiMt + Ilm	best fit (1)	1013–1070 ^b	0.0 ⁱ	–0.5 ^m		
H96A	icelandite	Ol + Aug + TiMt + Ilm	500	878–967	–0.58	–1.1	e	
H128	olivine tholeiite	Ol + Aug + Pig + TiMt + Ilm	best fit (1)	1011–1088 ^b	0.15 ^u	–0.18 ^u		
Witu (Papua New Guinea)								
16	dacite	Opx + Aug + TiMt + Ilm	(1000–5000)	1015–1040 ^b	0.6–0.7 ^r	0.4–0.6 ^g		12
20	rhyodacite	Opx + Aug + TiMt + Ilm	(1000–5000)	940–1015 ^b	0.9–1.1 ⁱ	0.0–0.1 ^g		
24	basalt	Ol + Opx + Aug + TiMt	(1000–5000)	1040–1070 ^b	1.2–1.3 ⁱ	0.9–1.2 ^g		
29	andesite	Ol + Pig + Aug + TiMt + Ilm	(1000–5000)	1040–1070 ^b	1.9–2.1 ⁱ	0.9–1.1 ^g	p	

Note: Maximum and minimum f_{O_2} are relative to the FMQ buffer at the indicated temperature and pressure. Letter designations are as follows: a = pressures in brackets were imposed on the calculations, those not in brackets were calculated from the assemblage; b = temperature from pyroxene thermometer; c = $\Delta \log f_{O_2}$ from OUOpA; d = $\Delta \log f_{O_2}$ from OpAUQ; e = oxides and pyroxenes give similar temperatures, and thus f_{O_2} range comes from the oxides; f = $\Delta \log f_{O_2}$ from QUIIP; g = $\Delta \log f_{O_2}$ from OpAUQ; h = $\Delta \log f_{O_2}$ from displaced OpUIO; i = calculations assume that magnetite composition did not change by more than 0.01 mol% ulvöspinel during cooling, results provide minimum T and minimum f_{O_2} ; j = $\Delta \log f_{O_2}$ from QUIIP; k = calculations assume that oxides and silicates are in equilibrium; l = pressure from K42 and K139; m = lower limits to f_{O_2} from ilmenite composition; n = see Lindsley et al. (1990); o = absence of pigeonite restricts temperature to <1085 °C at 1 kbar and <1127 °C at 3 kbar; p = olivine is not in equilibrium with the pyroxenes, it is assumed to be xenocrystic, $\Delta \log f_{O_2}$ will be close to the lower limits shown in the table if olivine is stable; q = high f_{O_2} limit is the oxidation of titaniferous magnetite of given composition to ilmenite; r = from Frost et al. (1988); s = see text; t = $\Delta \log f_{O_2}$ from QUIIP; u = $\Delta \log f_{O_2}$ from ApUIO; v = upper limits of f_{O_2} from composition of titaniferous magnetite. References: 1 = Hildreth (1977); 2 = Brophy (1984); 3 = Brophy (1986); 4 = Druitt and Bacon (1989); 5 = Bizouard et al. (1980); 6 = Hildreth (1983); 7 = Ewart et al. (1971); 8 = Ewart et al. (1975); 9 = Ewart (personal communication); 10 = Singer et al. (1992); 11 = Carmichael (1967a); 12 = Johnson and Arculus (1978).

0.90 in the well-constrained tholeiite and 0.85–1.0 in the basaltic andesites, to 0.99–1.0 in the icelandite and rhyolite. Thus, although the uncertainties are relatively large and mainly overlapping, these values do suggest an increase in a_{SiO_2} with Fe enrichment.

Other volcanic suites

Oxide and pyroxene thermometry for a number of other volcanic centers are summarized in Table 2 and Figure 5. In the few rocks for which the oxide and pyroxene thermometers give similar results, the reported temperature is that which is compatible with both the oxide and pyroxene thermometers and with pyroxene QUIIF equilibria. In the many samples for which the oxides and pyroxenes do not agree, the oxides always give temperatures lower than those indicated by the pyroxenes. In these instances we use the pyroxene temperature and delimit f_{O_2} by the use of pyroxene QUIIF equilibria (see Table 2; Lindsley and Frost, 1992, for the calculation schemes used). For a few samples we were able to calculate pressure directly, but for most we had to hold pressure fixed because the assemblages do not adequately constrain pressure. If the analyses came from groundmass phases

we assumed that the pressure is 1 bar; otherwise we used a pressure range of 1000–5000 bars.

Figures 5A–5C show that most of the suites crystallized at nearly the same relative f_{O_2} (about 1–2 log units above FMQ, or around that of the Ni–NiO buffer). It is noteworthy that within each volcanic center the more primitive rock types reflect higher temperatures than do the more evolved ones. For example, andesites of Seguam crystallized at higher temperature than did the dacites. However, there is no consistency in temperature among the various eruptive centers. For example, the dacites from Seguam formed at the same temperatures as the andesites of Cold Bay. This probably reflects different intensive parameters—most likely f_{H_2O} —among the eruptive centers, an inference supported by the presence of amphibole in the more evolved Cold Bay rocks and its absence from those of Seguam. (The classification of Seguam rocks is ambiguous. We treat them as calc-alkalic because the basalts lack the classical petrographic requisite of tholeiites, low-Ca pyroxene.)

An important point is that for a large number of suites the oxides give lower temperatures than do the pyroxenes. We interpret this fact as showing that the oxides in volcanic rocks generally continue to reequilibrate until

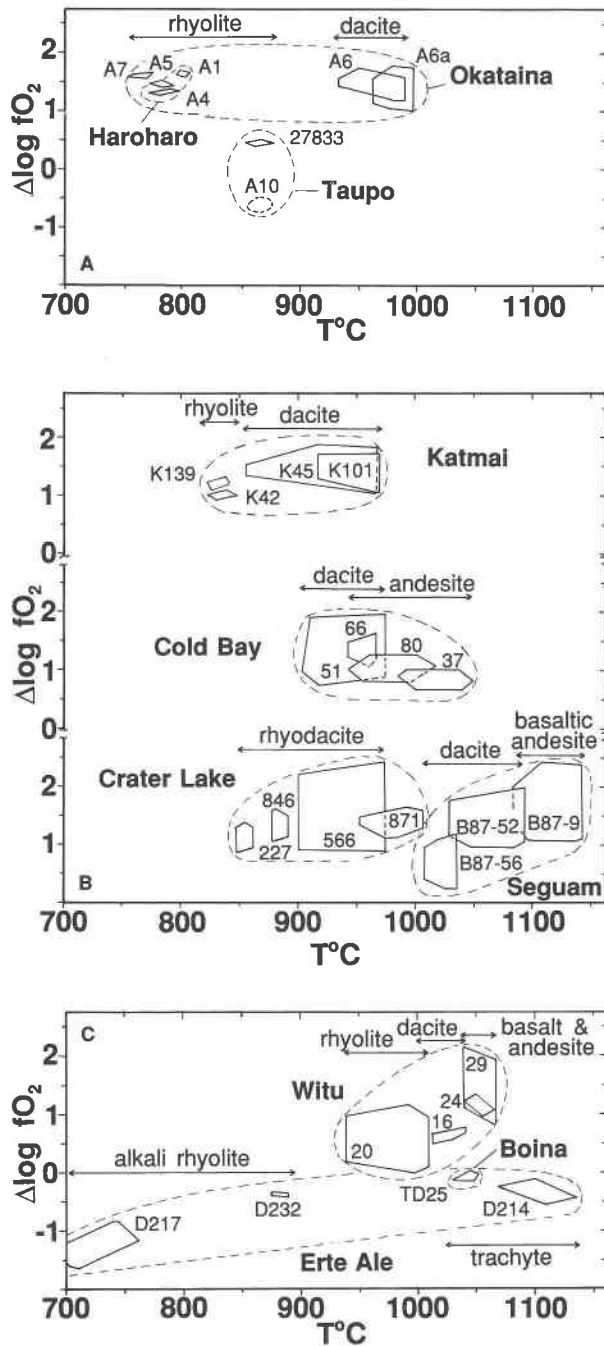


Fig. 5. Diagrams of $\Delta \log f_{O_2}$ vs. T showing equilibrium conditions for various volcanic rocks, as calculated from QUIIF equilibria. (A) New Zealand rhyolites. (B) Katmai, Cold Bay, Crater Lake, and Seguam. (C) Witu, Erta Ale, and Boina. Data and references from Table 2.

the final melt in the rock freezes. As a result, the final oxide composition may not be in equilibrium with the silicates or may be in equilibrium with only the most Fe-rich rims of the pyroxenes and olivines.

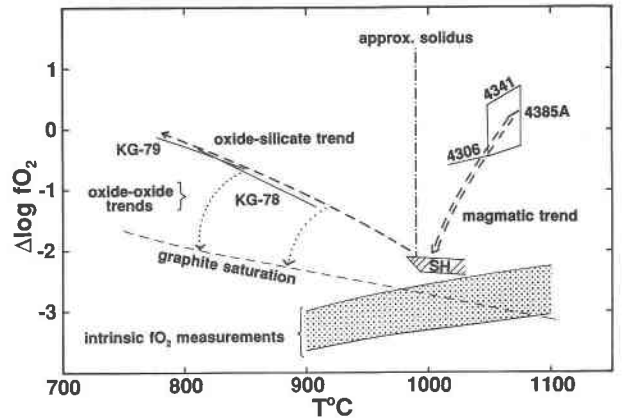


Fig. 6. A diagram of $\Delta \log f_{O_2}$ (FMQ) vs. T showing the f_{O_2} during the crystallization of the Skaergaard Intrusion. Sample numbers for LZb (4385A), MZ (4341), and UZa (4306) are from Brown (1957), and those for the Upper Border Group (UBG; KG-78 and KG-79) are from Naslund (1980). Shaded band shows the f_{O_2} for the Skaergaard inferred from intrinsic f_{O_2} measurements (Sato and Valenza, 1980). Double-dashed arrow shows the probable f_{O_2} trend during magmatic crystallization, single-dashed arrow shows oxide-silicate trend in the UBG, and dotted arrows show possible oxide-oxide cooling trends.

PLUTONIC ROCKS

The Skaergaard Intrusion

Because pressure is tightly constrained in the Skaergaard, one can use the pyroxene QUIIF approach to calculate the f_{O_2} conditions for formation much as we did for volcanic rocks. The f_{O_2} of the Skaergaard has been the subject of considerable study (Buddington and Lindsley, 1964; Lindsley et al. 1969; Williams, 1971; Morse et al. 1980; Sato and Valenza, 1980). The results are disparate: Sato and Valenza (1980) suggested that the Skaergaard crystallized in the range of the IW buffer, whereas other studies indicate f_{O_2} much closer to FMQ for much of the igneous history. The pyroxene QUIIF approach provides a way to settle this dispute, for it allows us to calculate f_{O_2} in those horizons that have low-variance assemblages, even though the oxide compositions may have completely reset. All that is needed to calculate f_{O_2} is the fact that oxides were present in the rock, for only a limited range of oxide compositions can have been in equilibrium with the silicates.

We have calculated the crystallization conditions in five horizons of the Skaergaard Intrusion: (1) Lower Zone b (sample 4385A), below the olivine hiatus, (2) the Middle Zone (sample 4341), where olivine is absent, (3) Upper Zone a (sample 4306), when olivine reappears and low-Ca Px is still stable, (4) the Sandwich horizon (sample 4471), and (5) Upper Border Group (samples KG-78, KG-79), where quartz occurs with fayalite and hedenbergite (Fig. 6). The conditions for the Sandwich horizon (SH in Fig. 6) were taken from Frost et al. (1988). The ferromagnesian silicates in these rocks are not in Fe-Mg exchange equilibrium, which probably reflects the incom-

plete exchange of Fe and Mg during cooling. Figure 6 thus shows the range of temperatures consistent with the range of Fe-Mg ratios found in ferromagnesian silicates of each rock.

Sample KG-78 is instructive. The oxides alone give a temperature of 573–615 °C, with $\Delta \log f_{\text{O}_2} = -0.46$ to -1.34 . These conditions clearly represent subsolidus re-equilibration, as was noted by Naslund (1984). Application of QUIIF equilibria can help us recover primary compositions. Frost et al. (1988) applied the original QUIIF equilibrium (without augite) and derived a maximum temperature of 970–1020 °C, under the assumption that the ilmenite ($X_{\text{Hem}} = 0.028$) had retained its original composition and that the titaniferous magnetite had lost much of its FeTiO_4 component by oxidation. If augite is included, there are 21 equilibria among the phases, and 11 are independent. The lowest temperature at which all these phases can have been in equilibrium, assuming that X_{La} and $X_{\text{Wg}}^{\text{Aug}}$ did not change, is shown in Figure 6: 810–910 °C. If those phases did exchange Ca upon cooling, we calculate temperatures similar to those inferred by Frost et al. (1988); X_{La} and $X_{\text{Wg}}^{\text{Aug}}$ would have changed from 0.021 to the present 0.015 and from 0.387 to 0.415, respectively.

It is evident from Figure 6 that the Skaergaard magma underwent strong relative reduction during differentiation from f_{O_2} near FMQ to values as much as 2 log units below (double-dashed arrow in Fig. 6), with the lowest relative f_{O_2} occurring in the most Fe-enriched portion, the Sandwich horizon. The rocks of the Upper Border Group clearly underwent subsolidus re-equilibration along the QUIIF equilibrium (Frost et al., 1988). At no point in the magmatic history of the intrusion could the f_{O_2} have been as low as that suggested by the whole-rock intrinsic f_{O_2} measurements (Sato and Valenza, 1980). Regardless of any uncertainty in the calculations above, reference to Figure 3 in Lindsley and Frost (1992) shows that Opx + titaniferous magnetite simply cannot be stable at the extremely low f_{O_2} Sato and Valenza (1980) suggested for the crystallization of the Skaergaard.

In rocks where the oxides remained in equilibrium with the silicates after solidification, such as in the UBG, the f_{O_2} of the fluids would have followed the QUIIF equilibrium with consequent oxidation (single dashed arrow in Fig. 6). Once the oxide-silicate equilibria closed, the f_{O_2} of the fluid would then have been controlled by the interoxide equilibria, probably resulting in relative reduction (dotted arrows, Fig. 6; Frost et al., 1988; Fuhrman et al., 1988), although a path at constant $\Delta \log f_{\text{O}_2}$ is also possible. If the magmatic fluids in the Skaergaard were carbonic, then the reduction would have led to the precipitation of grain-boundary graphite, similar to that of mafic rocks from the Laramie Anorthosite Complex (Frost et al., 1989). This may be the key to the discrepancy between the f_{O_2} estimated from mineral equilibria and from intrinsic measurements. Sato and Valenza (1980) noted that some of their samples underwent autoreduction during heating; they ascribed this to the presence of

graphite. The graphite inferred by Sato and Valenza (1980) cannot have been magmatic but may have precipitated during cooling. Note that the conditions considered here range from magmatic to high subsolidus. The massive flooding with hydrothermal fluid suggested by O and H isotopic studies (e.g., Taylor and Forester, 1979) must have occurred later, at distinctly lower temperatures.

Other mafic plutons

Most plutonic rocks are not suitable for the detailed treatment we have shown for volcanic rocks and the Skaergaard Intrusion, for typically the silicates, as well as the oxides, have reset their compositions through exsolution, subsolidus exchange, and similar processes. Accordingly, we have chosen to show their relations on a petrogenetic grid. Fortunately, the most critical compositional parameter is Fe^{2+}/Mg in the silicates. Accordingly, we have plotted plutonic examples on isobaric diagrams of $\Delta \log f_{\text{O}_2}$ vs. $X_{\text{Fe}^{\text{Opx}}}$ (Figs. 7–10). Note that, even if Opx is absent, we can still plot the compositional parameter by calculating the Opx that would be in Fe-Mg exchange equilibrium with the other phases. We chose 3 kbar because many plutonic rocks probably crystallized within 1 or 2 kbar of that value. For pyroxene-bearing felsic rocks (such as charnockites), the net (Fig. 10) is isothermal at 800 °C, because many charnockitic rocks form near that temperature (Janardhan et al., 1982; Bhattacharya and Sen, 1986). For most other plutonic suites, an isothermal diagram is unsuitable. Accordingly, Figures 7–9 are polythermal; temperature varies linearly with $X_{\text{Fe}^{\text{Opx}}}$: 1200 °C for $X_{\text{Fe}^{\text{Opx}}} = 0$, 1100 °C for 0.5, and 1000 °C for 1.0. We estimate that this simplified temperature scale is accurate to within ± 50 °C. For example, 1200 °C is near the 1-atm liquidus for basaltic rocks (Basaltic Volcanism Study Project, 1981), and basaltic magmas come to the surface near that temperature (Wright et al., 1968). Fe-rich residua of mafic plutons commonly crystallize near 1000 °C: 950–1030 °C for the Skaergaard Sandwich horizon (Lindsley et al., 1969), ~ 960 °C for late liquids in the Kiglapait (Morse, 1980), 980–1030 °C for Fe-rich rocks of the Sybille Monzosyenite (Fuhrman et al., 1988). The main purpose of Figures 7–9 is to show relative $\Delta \log f_{\text{O}_2}$ for various assemblages and rock types. Neither the fixed pressure nor the simplified temperature scale introduces significant errors for magnesian and intermediate compositions. Errors are larger for Fe-rich suites for two reasons: first, the reaction $\text{Opx} = \text{Ol} + \text{SiO}_2$ is sensitive to pressure; and, second, the location of the QUIIF curve in $\Delta \log f_{\text{O}_2}$ vs. $X_{\text{Fe}^{\text{Opx}}}$ space is rather strongly temperature dependent. Thus one must be careful when comparing Fe-rich rocks that may have formed at significantly different pressures. A further simplification of Figures 7–9 is the treatment of all low-Ca pyroxene as Opx. Figures 3D, 3E, and 3H of Lindsley and Frost (1992) show that this step introduces errors of 0.0–0.2 log units in $\Delta \log f_{\text{O}_2}$ for pigeonite-bearing rocks.

We use this petrogenetic net (Figs. 7–9) to illustrate the way that common assemblages among olivine, pyrox-

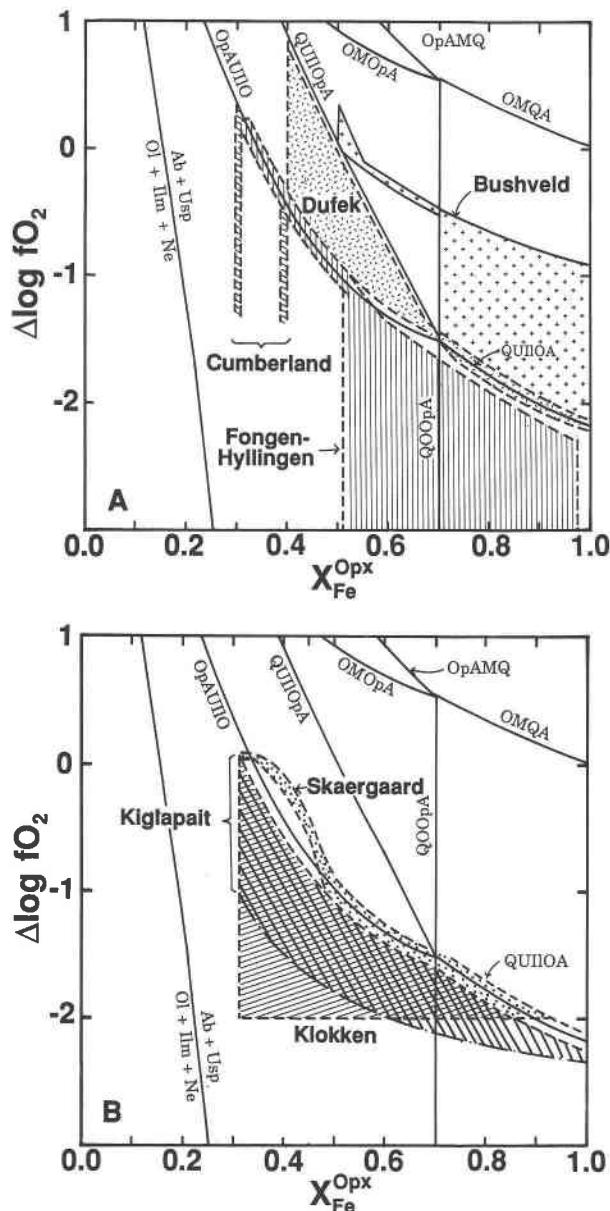


Fig. 7. Polythermal diagrams of $\Delta \log f_{O_2}$ (FMQ) vs. X_{Fe}^{Opx} (at 3000 bars) showing trends for mafic plutons of tholeiitic affinity. Abbreviations as in Table 1. (A) Bushveld, Cumberland, Dufek, and Fongen-Hyllingen. (B) Skaergaard, Kiglapait, and Klokken. Data and references from Table 4. Figures 7–9 show the curve $NaAlSi_3O_8$ (Ab) + $4 Fe_2TiO_4$ (Usp) = $NaAlSi_3O_4$ (Ne) + $2 Fe_2SiO_4$ (Ol) + $4 FeTiO_3$ (Ilm) which marks the lower f_{O_2} limit of the assemblage plagioclase + TiMt + olivine. It uses a_{SiO_2} from albite-nepheline (Carmichael et al., 1974, revised to the standard state of quartz) to displace QUIIOA.

enes, Fe-Ti oxides, and quartz are related (Table 3). If the assemblage is of suitably low variance (such as assemblages in field 1, Table 3), the f_{O_2} of a suite of rocks appears as a line in the projections, with the f_{O_2} simply determined by X_{Fe}^{Opx} . In assemblages of higher variance (i.e., assemblages 2–9 in Table 3), the crystallization conditions appear as fields. For assemblages 2–4, the upper

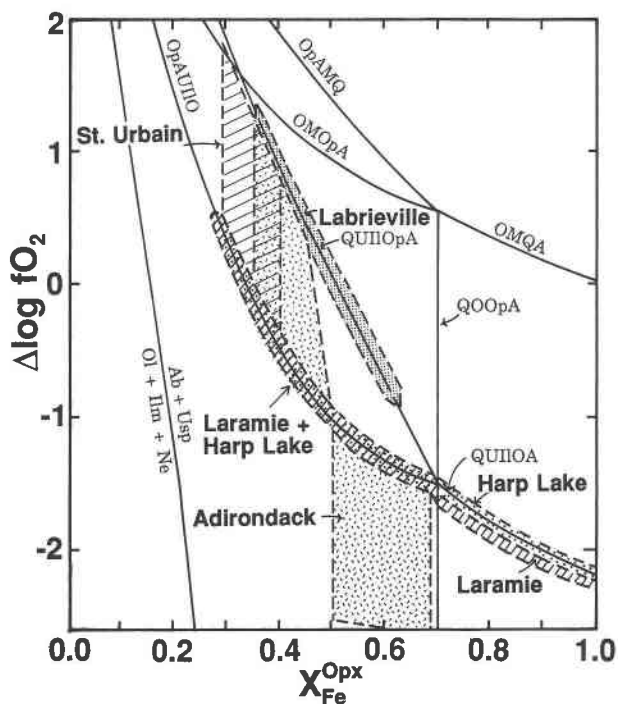


Fig. 8. Polythermal diagram of $\Delta \log f_{O_2}$ (FMQ) vs. X_{Fe}^{Opx} (at 3000 bars) showing the crystallization trends of anorthositic plutons: Adirondack, Harp Lake, Labrieville, Laramie, and St. Urbain. Data and references from Table 5. Abbreviations as in Table 1.

f_{O_2} limits of the field are determined by titaniferous magnetite-bearing buffer surfaces. If N_{Ti} is known or can be estimated, then the field can be further limited by displacing the buffering assemblages according to the titaniferous magnetite composition. Fields for assemblages 6–9 are bounded by isopleths of ilmenite composition. Ilmenite tends to become poorer in Fe^{3+} during cooling, so the most Fe_2O_3 -rich ilmenite found in an assemblage will be closest to the composition of the primary ilmenite. The ilmenite isopleth from the two-oxide thermometer will therefore be the low- f_{O_2} limit for the assemblage.

These diagrams permit us to compare the crystallization paths of some of the best-known mafic intrusions of tholeiitic (Fig. 7; Table 4), anorthositic (Fig. 8; Table 5), and calc-alkalic (Fig. 9) affinity. Perhaps the most striking feature is the difference between tholeiitic and calc-alkalic mafic plutons (Table 6). Magnetite and ilmenite appear in plutons of the tholeiitic affinity where the fictive X_{Fe}^{Opx} is between 0.3 and 0.4. The plutons are marked by a distinct Fe-enrichment trend that in many instances results in assemblages containing nearly pure fayalite. Mafic calc-alkalic plutons differ from the tholeiitic plutons in that magnetite, often without ilmenite, first appears in rocks that are distinctly more magnesian ($X_{Fe}^{Opx} = ca. 0.2$) (Figs. 9A, 9B). A more important and possibly correlative feature is the fact that, unlike most mafic plutons of tholeiitic affinity, calc-alkalic layered mafic plutons do not show a monotonic increase in X_{Fe}^{Opx} as one moves stratigraphically upward. Instead Fe-enrichment trends may

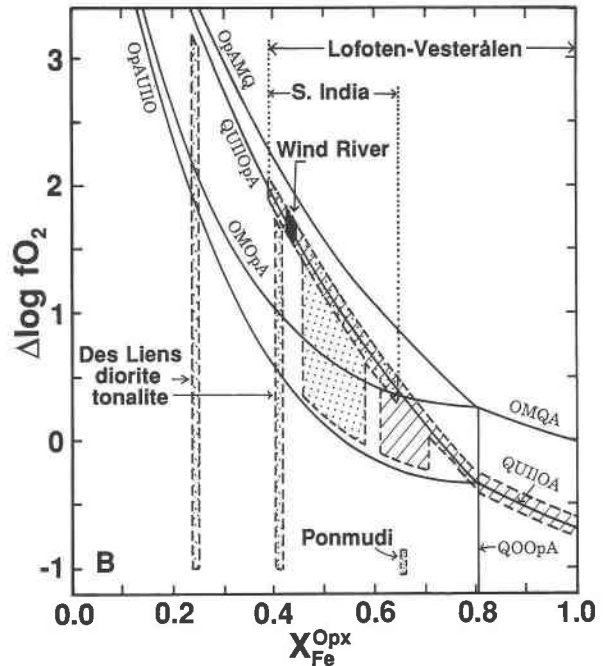
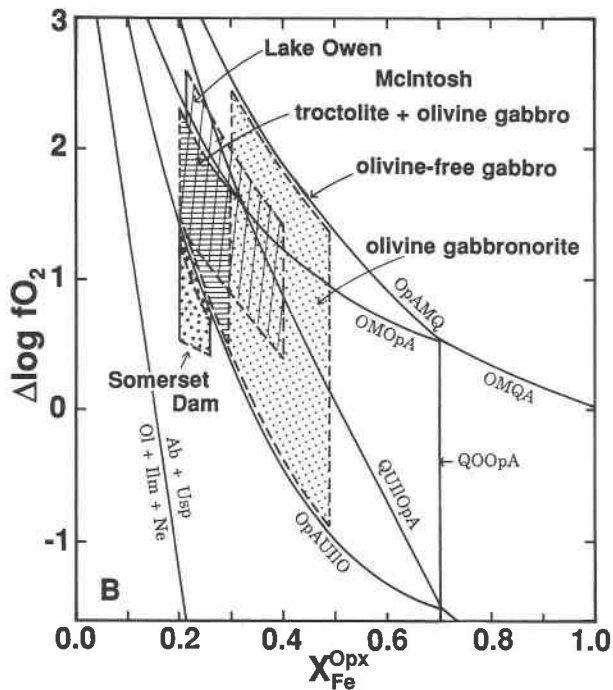
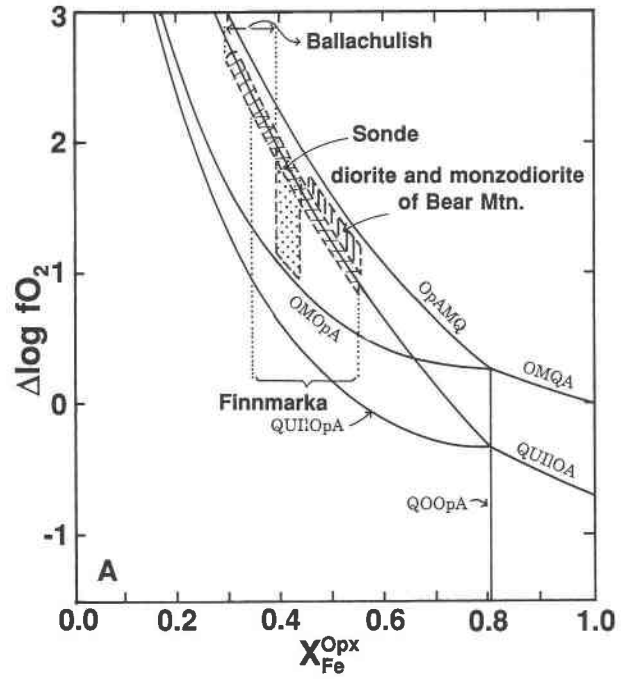
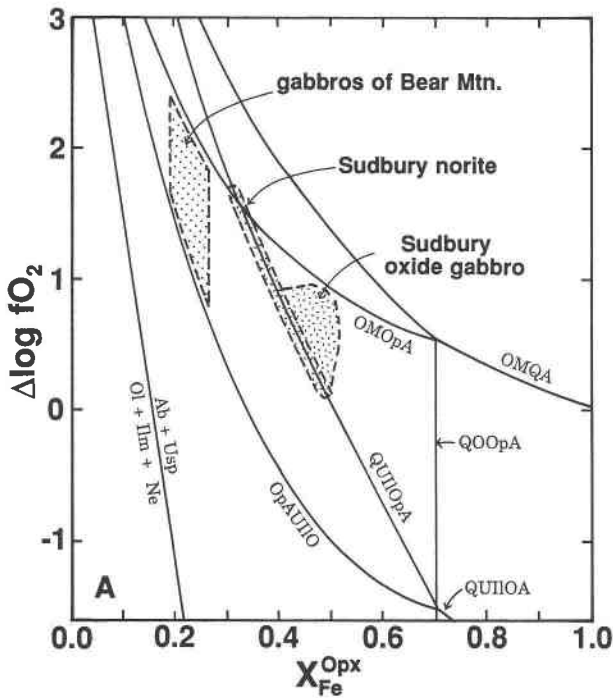


Fig. 9. Polythermal diagrams of $\Delta \log f_{O_2}$ (FMQ) vs. X_{Fe}^{Opx} (at 3000 bars) showing the crystallization trends of mafic plutons of calc-alkalic affinity. Abbreviations as in Table 1. (A) Trends for gabbros of the Bear Mountain complex and Sudbury irruptive. (B) Trends for Lake Owen, McIntosh, and Somerset Dam intrusions. Data and references from Table 6.

Fig. 10. A diagram of $\Delta \log f_{O_2}$ (FMQ) vs. X_{Fe}^{Opx} diagram for 800 °C and 3000 bars showing the crystallization trends of pyroxene-bearing felsic rocks. Abbreviations as in Table 1. (A) Trends for Ballachulish, the Bear Mountain (diorite and monzodiorite), Finnmarka, and Sonde. (B) Trends for Des Liens complex, Lofoten-Vesterålen, Ponmudi, and southern India. Data and references from Table 7.

be interrupted by gentle Mg-enrichment trends up to a kilometer thick or by abrupt increases in Mg with increasing stratigraphic height. Perhaps as a result of these reversals, calc-alkalic layered mafic plutons do not attain

the extreme enrichment so characteristic of most layered tholeiitic mafic plutons.

Clearly, calc-alkalic mafic plutons are more oxidized than tholeiitic plutons. Calc-alkalic plutons crystallized

TABLE 3. Information deduced from the petrogenetic net for pyroxenes and Fe-Ti oxides with olivine or quartz

Assemblage	Data needed	Information
1 Q + Ol + (Aug) + TiMt + Ilm Ol + Opx + (Aug) + TiMt + Ilm Q + Opx + (Aug) + TiMt + Ilm	X_{Fe}^{Opx} (from X_{Fe}^{Ol} if necessary)	Relative f_{O_2} of crystallization
2 Q + Opx + (Aug) + TiMt	X_{Fe}^{Opx} (N_{Ti})	Max f_{O_2} = OpAMQ Min f_{O_2} = OMOpA or QUIOpA; a
3 Ol + Opx + (Aug) + TiMt	X_{Fe}^{Opx} (N_{Ti})	Max f_{O_2} = OMOpA Min f_{O_2} = OpAUIIO; a
4 Q + Ol + (Aug) + TiMt	X_{Fe}^{Opx} from X_{Fe}^{Ol} ; (N_{Ti})	Max f_{O_2} = OMQA Min f_{O_2} = QUIIOA; a
5 Opx + (Aug) + TiMt + Ilm	X_{Fe}^{Opx} ; (N_{Ti}) (X_{Hem})	Max f_{O_2} = QUIOpA; a, b Min f_{O_2} = OpAUIIO; a, b
6 Ol + (Aug) + TiMt + Ilm	X_{Fe}^{Opx} from X_{Fe}^{Ol} ; X_{Hem} ; (N_{Ti})	Max f_{O_2} = OpAUIIO; a Min f_{O_2} = X_{Hem} isopleth
7 Opx + (Aug) + Q + Ilm	X_{Fe}^{Opx} ; X_{Hem}	Max f_{O_2} = QUIOpA Min f_{O_2} = X_{Hem} isopleth
8 Ol + (Aug) + Q + Ilm	X_{Fe}^{Opx} from X_{Fe}^{Ol} ; X_{Hem}	Max f_{O_2} = QUIIOA Min f_{O_2} = X_{Hem} isopleth
9 Ol + Opx + (Aug) + Ilm	X_{Fe}^{Opx} ; X_{Hem}	Max f_{O_2} = OpAUIIO Min f_{O_2} = X_{Hem} isopleth

Note: a = limits can be further constrained with N_{Ti} ; b = with X_{Hem} .

at $\Delta \log f_{O_2}$ of 1–2 (except for the rare oxide-rich layers of the McIntosh intrusion that may have formed at f_{O_2} values as much as 1 log unit below FMQ), whereas crystallization of magnetite in most tholeiitic plutons begins at f_{O_2} near FMQ and falls with Fe enrichment to values well below FMQ ($\Delta \log f_{O_2} = -1$ to -2).

In many respects anorthositic plutons (Fig. 8; Table 5) behave much like the tholeiitic intrusions mentioned above. Most show a distinct Fe-enrichment trend. We consider them as a separate category here because it is by no means clear whether anorthosite complexes, which are moderately alkalic, are actually related to tholeiitic magmatism. A distinctive feature about anorthositic rocks is the wide range of f_{O_2} that they display. Labrieville and St. Urbain are marked by relatively oxidized hemoilmenites (Anderson, 1966; Dymek and Gromet, 1984), where-

as the ilmenite from the Adirondack, Laramie, and Harp Lake anorthosite bodies is distinctly low in Fe^{3+} . The different f_{O_2} conditions of these bodies may reflect differences inherent in the parent melts or may simply reflect higher degrees of crustal assimilation, and hence higher silica activity, in the St. Urbain and Labrieville bodies.

The topologies shown in Figures 7–9 are also important in understanding the evolution of intensive parameters within a single pluton. During closed-system crystallization of a pluton, once a low-variance assemblage (QUIOpA, OpAUIIO, or QUIIOA) has been attained, one would expect that, because of the low abundance of free O_2 , the buffering assemblage would be maintained during continued closed-system crystallization. Thus, excursions from a buffering assemblage would have important implications for the evolution of a pluton. We can

TABLE 4. Mineral assemblages in mafic plutons of tholeiitic affinity

Locality	Assemblage	X_{Fe}^{Opx} *	Reference
Bushveld	Opx + Aug + TiMt	0.50–0.55	1, 2, 3
	Opx + Aug + Ol + TiMt	0.55–0.70	
	Ol + Aug + TiMt	0.70–1.00	
Cumberland	Ol + TiMt + Ilm	$N_{Ti} = 0.37$ –0.52	4
	Ol + Aug + TiMt + Ilm	0.31	
		0.38	
Dufek	Opx + Aug + TiMt + Ilm	$X_{Hem} = 0.05$ –0.06	5, 6
	Q + Opx + Aug + TiMt + Ilm	0.40–0.52	
	Q + Aug + (Ol?) + TiMt + Ilm	0.52–0.71	
Fongen-Hyllingen	Ol + Opx + Aug + TiMt + Ilm	0.71–0.75	7, 8
	Ol + Opx + Aug + TiMt + Ilm	0.32–0.51	
	Ol + Opx + Aug + Ilm	0.51–1.00	
Kiglapait	Ol + Aug + TiMt + Ilm	0.32–1.00	9, 10
	Ol + Aug + TiMt + Ilm	0.40–0.92	
	Q + Ol + Aug + TiMt + Ilm	0.92–0.95	
Skaergaard	Ol + Opx + Aug + Ilm	0.33–0.37	12, 13, 14, 15
	Opx + Aug + TiMt + Ilm	0.37–0.48	
	Ol + Opx + Aug + TiMt + Ilm	0.48–0.57	
	Ol + Aug + TiMt + Ilm \pm Q	0.57–1.00	

Note: References: 1 = Atkins (1969); 2 = Willemsse (1969); 3 = Molyneux (1972); 4 = Rutherford (1984); 5 = Himmelberg and Ford (1976); 6 = Himmelberg and Ford (1977); 7 = Thy (1982); 8 = Wilson et al. (1981); 9 = Morse (1979); 10 = Morse (1980); 11 = Parsons (1981); 12 = Vincent and Phillips (1954); 13 = Wager and Brown (1968); 14 = Naslund (1984); 15 = Brown (1957).

* Calculated from another iron magnesium silicate if Opx is absent.

TABLE 5. Mafic plutons of anorthositic affinity

Locality	Assemblage	Range in $X_{Fe}^{Opx^*}$	Reference
Adiron- dacks	Opx + Aug + TiMt + Ilm	0.35–0.46	1
	Ol + Opx + Aug + TiMt + Ilm	0.50	
	Ol + Aug + TiMt + Ilm	0.63–0.64	
Harp Lake	Ol + Opx + Aug + TiMt + Ilm ^a	0.25–0.80	2
	Ol + Aug + Q + TiMt + Ilm ^b	0.80–0.98	
Labrieville	Opx + Aug + Q + TiMt + Ilm ^c	0.37–0.65	3
Laramie	Ol + Opx + Aug + TiMt + Ilm ^a	0.30–0.80	4, 5
	Ol + Aug + Q + Ilm ^d	0.80–1.00	
St. Urbain	Opx + Aug + TiMt + Ilm ^e	0.29–0.40	6

Note: a = in anorthosite and ferrodiorite; b = in adamellite; c = in anorthosite; d = in monzonitic rocks. References: 1 = Ashwal (1982); 2 = Emslie (1980); 3 = Anderson (1966); 4 = Fuhrman et al. (1988); 5 = Frost et al. (1992); 6 = Dymek and Gromet (1984).

* Calculated from another iron magnesium silicate if Opx is absent.

postulate several causes for such an excursion. One is simply the peritectic reaction of olivine to Opx. In the presence of two oxides, that would cause the assemblage to move off the OpAUlIO buffering surface into the two pyroxene–two oxide field. Such an excursion apparently happened during the evolution of the Skaergaard Intrusion. The second type of excursion, which typically involves an increase in Mg as well as a change in the buffering assemblage, is common in the calc-alkalic intrusions, where it is well represented in rocks from Lake Owen (Patchen, 1987) and from Somerset Dam (Mathison, 1967, 1975). It is best interpreted as reflecting injection of new magma into the intrusion. The third type of excursion occurs at high Fe enrichment, whereby magnetite reacts out, leaving a crystallizing assemblage of olivine, ilmenite, and quartz, as in the monzonites of the Laramie Anorthosite Complex (Fuhrman et al., 1988) and in the Fongen-Hyllingen intrusion. Fuhrman et al. (1988) interpret this as a reflection that the f_{O_2} was controlled by a graphite + fluid equilibrium, rather than by reactions among oxides and iron magnesium silicates.

Despite the obvious problems inherent in projecting relations from four dimensions into two, our polythermal projection can be valuable in comparing the crystallization conditions of mafic plutons. One reason is because the f_{O_2} of melts is generally controlled internally rather

than externally (Carmichael, 1991). Thus, a melt of the composition of the Sudbury irruptive, for example, will have followed a path of T vs. $\Delta \log f_{O_2}$ governed by the assemblage of QUIIOp, regardless of the P - T conditions of final crystallization. What these diagrams compare, therefore, is the relative location of the various buffering assemblages found in a suite of rocks, rather than simply the absolute $\Delta \log f_{O_2}$ and T at which the rocks crystallized. In other words, these diagrams show the differences in $\Delta \log f_{O_2}$ that would be followed by various mafic intrusions if they had been subjected to the same pressure and temperature ranges of crystallization.

Pyroxene-bearing felsic rocks

An isobaric, isothermal diagram of $\Delta \log f_{O_2}$ vs. X_{Fe}^{Opx} is useful to show crystallization trends in pyroxene-bearing felsic rocks (Figs. 10A, 10B; Table 7). The rocks discussed here include those pyroxene-bearing rocks that form the mafic portions of some calc-alkalic plutons as well as charnockitic rocks, that is, pyroxene granites and granodiorites associated with granulite complexes.

One striking feature of the pyroxene-bearing (or olivine-bearing) felsic rocks is the wide range of compositions (and hence f_{O_2}) that they cover. Since most of these rocks contain two oxides + quartz, the f_{O_2} can be directly related to X_{Fe}^{Opx} (which ranges from around 0.3 to values of nearly 1.0). The significance of this wide range in composition is not clear. It is not likely to reflect simple Fe enrichment during differentiation, for the two areas that show the widest range of values, southern India and Lofoten-Vesterålen, contain numerous charnockitic plutons that may well be unrelated to each other. Furthermore, in at least one pluton, Finnmarka, differentiation is associated with a decrease in X_{Fe} in the silicates and hence increases in f_{O_2} (Czamanske and Wones, 1973).

Another interesting set of pyroxene-bearing felsic rocks are those that lack magnetite, the Des Liens complex and Ponmudi. Oxide-silicate equilibria can set only a maximum f_{O_2} for these rocks. Of particular significance is Ponmudi, which is graphite bearing; it formed at f_{O_2} at least an order of magnitude below those required for the stability of magnetite.

TABLE 6. Mafic plutons of calc-alkalic affinity

Location	Assemblage	$X_{Fe}^{Opx^*}$	Reference
Bear Mountain Lake Owen	Ol + Opx + Aug + TiMt	0.23–0.27	1
	Opx + Aug + TiMt	0.22–0.40	2
McIntosh	Ol + Aug + Opx + TiMt troct.; ol. gab. gabbro norite oxide gabbro norite	$X_{Usp} = 0.32$ –0.41	3
		0.20–0.24	
		0.35	
Somerset Dam	Ol + Aug + Opx + TiMt + Ilm	0.20–0.32	4, 5
	Ol + Aug + TiMt + Ilm	0.22–0.25	
Sudbury	Q + Opx + Aug + TiMt + Ilm	0.31–0.38	6
	Q + Aug + TiMt + Ilm	0.43–0.48	

Note: References: 1 = Snoke et al. (1981); 2 = Patchen (1987); 3 = Mathison and Hamlyn (1987); 4 = Mathison (1967); 5 = Mathison (1975); 6 = Naldrett et al. (1970).

* Calculated from another iron magnesium silicate if Opx is absent.

TABLE 7. Felsic plutonic rocks with pyroxenes

Location	Assemblage	X_{Fe}^{Opx*}	Rock type	Reference
Ballachulish	Opx + Aug + (Q) + TiMt + Ilm	0.30–0.38	monzodiorite	1, 2
	Q + Aug + Opx + Aug	0.30–0.38	q. diorite	
Bear Mountain Des Leins	Opx + Aug + TiMt	0.45–0.56	monzodiorite	3
	Q + Opx + Aug + Ilm	0.41–0.42	tonalite	
Finnmarka Lofoten-Vesterålen	Q + Opx + Aug + Ilm	0.24	diorite	5, 6
	Q + Opx + Aug + TiMt + Ilm	0.35–0.55	monzonite	
	Opx + Aug + TiMt + Ilm	0.62–0.70	mafic mangerite	
	Q + Opx + Aug + TiMt + Ilm	0.4–0.8	mangerite	
Madras	Q + Fay + Aug	0.8–0.99	charnockite	8
	Opx + Aug + TiMt + Ilm	0.46–0.57	norite, diorite	
	Q + Opx + Aug + TiMt + Ilm	0.38–0.64	charnockite	
	Q + Opx + TiMt + Ilm	0.43–0.60	charnockite	
Ponmudi Sande	Q + Opx + Ilm + graphite	0.66	charnockite	9
	Opx + Aug + TiMt + Ilm	0.40	larvakite	
Wind River	Opx + Aug + Q + TiMt + Ilm	0.39–0.46	(monzonite) larvakite	10
	Q + Opx + Aug + TiMt + Ilm	0.44–0.48	diorite-charnockite	
	Q + Opx + Aug + TiMt	0.44–0.48	charnockite	

Note: References: 1 = Weiss (1986); 2 = Weiss and Troll (1989); 3 = Snoko et al. (1981); 4 = Percival (1992); 5 = Czamanske and Mihalik (1972); 6 = Czamanske and Wones (1973); 7 = Malm and Ormaasen (1978); 8 = Howie (1955); 9 = Ravindra Kumar et al. (1985); 10 = Anderson (1984); 11 = B.R. Frost (unpublished data).

* Calculated from another iron magnesium silicate if Opx is absent.

DIFFERENCES BETWEEN CALC-ALKALIC AND THOLEIITIC MELTS

Data for the volcanic rocks are summarized in Figure 11, which has several distinctive features. One is that, in agreement with the suggestion of Osborn (1959), the calc-alkalic suites (New Zealand, Bishop, Crater Lake, Katmai, Cold Bay, Witu, and Seguam) lie at relatively high f_{O_2} (i.e., up to 2 log units above FMQ) that are distinct from those of the tholeiitic and alkalic suites (Thingmull and Erta Ale), which lie as much as two log units below FMQ. This difference in f_{O_2} can also be seen in the plutonic suites (compare Figs. 7 and 9): calc-alkalic plutons crystallize at f_{O_2} about 1–2 log units above FMQ, whereas tholeiitic plutons crystallize at f_{O_2} up to 2 log units below FMQ. The only pluton having assemblages that overlap the f_{O_2} difference between tholeiitic and calc-alkalic rocks is the McIntosh intrusion, which has a few oxide-rich ferrogabbros with Opx as Fe rich as 0.50, but which overall behaves as a calc-alkalic intrusion.

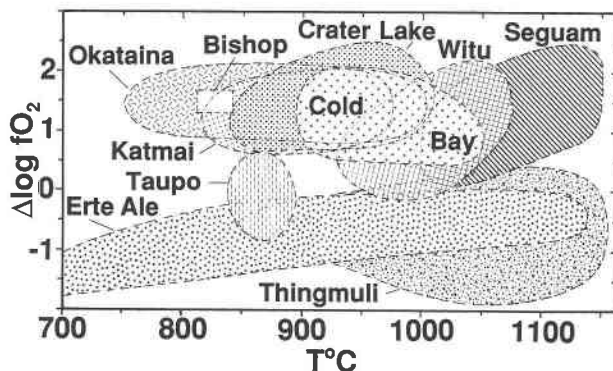


Fig. 11. Summary diagram of $\Delta \log f_{O_2}$ vs. T showing the crystallization conditions of the volcanic suites in Figures 4 and 5.

Figure 11 shows that, although Figures 7–10 suggest that Fe enrichment associated with differentiation should lead to decreases in relative f_{O_2} , such strong reduction is mainly lacking in most volcanic suites. Erta Ale does show a distinct decrease in relative f_{O_2} with decreasing temperature, and there is a hint of relative reduction in Seguam, Witu, and Crater Lake, but in general any change in relative f_{O_2} with decreasing temperature is smaller than the uncertainty of the f_{O_2} for each rock type within the suite.

An important aspect of oxide-silicate equilibria is that they give us insight into how differentiation of a melt affects f_{O_2} . Carmichael (1991) pointed out that decompression or assimilation of H_2O will not affect the f_{O_2} of a melt and argued that the f_{O_2} of a magma reflects the f_{O_2} of its source region. We contend that this conclusion is valid only if a melt has undergone little or no differentiation. If two oxides have crystallized from the melt in the presence of low-Ca pyroxene and either olivine or quartz, then, because the crystallizing assemblage will lie on an isobarically, isothermally univariant curve, Fe enrichment must involve relative reduction in the f_{O_2} of the melt. In some assemblages, however, Fe enrichment need not lead to relative reduction. For example, in an assemblage with fayalite, two oxides, and quartz it is possible for the relative reduction accompanying Fe enrichment to be balanced by relative oxidation inherent in falling temperature. Furthermore, if a crystallizing assemblage such as Opx + Cpx + Ilm + Mt lies in a field (rather than on a line) in Figures 7–9, a decrease in $\mu_{MgFe_{-1}}$ need not lead to any change in relative f_{O_2} because it can be accompanied by an increase in a_{SiO_2} or, if ilmenite is absent, by an increase in a_{TiO_2} .

ACKNOWLEDGMENTS

We are grateful to David Andersen and Paula Davidson for doing most of the development of the solution models and are especially indebted to

Andersen for producing the pyroxene QUILF program in a convenient form. We thank John Haas for providing his unpublished compilation of Fe-O-SiO₂, O₂ buffers and A. Ewart for providing unpublished analyses. We also thank Charlie Bacon, Pete Roeder, and Roger Nielsen for their perceptive reviews of an earlier version of this manuscript; their efforts have markedly improved its presentation. This work has been supported by NSF grants EAR-8720185 and EAR-8816040 to D.H.L. and EAR-8816604 to B.R.F., which we gratefully acknowledge. D.H.L. thanks the Department of Geology and Geophysics at the University of Wyoming for its support and hospitality during the fall semester, 1990, when most of this paper was written. Stony Brook Mineral Physics Institute publication no. 63.

REFERENCES CITED

- Andersen, D.J., Bishop, F.C., and Lindsley, D.H. (1991) Internally consistent solution models for Fe-Mg-Mn-Ti oxides: Part II, Fe-Mg-Ti oxides and olivine. *American Mineralogist*, 76, 427-444.
- Andersen, T. (1984) Crystallization history of a Permian composite monzonite-alkali syenite pluton in the Sande Cauldron, Oslo rift, southern Norway. *Lithos*, 17, 153-170.
- Anderson, A.T. (1966) Mineralogy of the Labrieville Anorthosite, Quebec. *American Mineralogist*, 51, 1671-1711.
- Ashwal, L.D. (1982) Mineralogy of mafic and Fe-Ti oxide-rich differentiates of the Marcy anorthosite massif, Adirondacks, New York. *American Mineralogist*, 67, 14-27.
- Atkins, F.B. (1969) Pyroxenes of the Bushveld Intrusion, South Africa. *Journal of Petrology*, 10, 222-249.
- Bacon, C.R., and Hirschmann, M.M. (1988) Mg/Mn partitioning as a test for equilibrium between coexisting Fe-Ti oxides. *American Mineralogist*, 73, 57-61.
- Basaltic Volcanism Study Project (1981) Basaltic volcanism on the terrestrial planets, 1286 p. Pergamon Press, New York.
- Bhattacharya, A., and Sen, S.K. (1986) Granulite metamorphism, fluid buffering, and dehydration melting in the Madras charnockites and metapelites. *Journal of Petrology*, 27, 1119-1141.
- Bizouard, H., Barberi, F., and Varet, J. (1980) Mineralogy and petrology of Erta Ale and Boina volcanic series, Afar Rift, Ethiopia. *Journal of Petrology*, 21, 401-436.
- Bohlen, S.R., and Essene, E.J. (1977) Feldspar and oxide thermometry of granulites in the Adirondack Highlands. *Contributions to Mineralogy and Petrology*, 62, 153-169.
- Brophy, J.G. (1984) The chemistry and physics of Alcutian arc volcanism. The Cold Bay volcanic center, southwestern Alaska. Ph.D. thesis, Johns Hopkins University, Baltimore.
- (1986) The Cold Bay volcanic center, Aleutian volcanic arc I: Implications for the origin of high-aluminum arc basalt. *Contributions to Mineralogy and Petrology*, 93, 368-380.
- Brown, G.M. (1957) Pyroxenes from the early and middle stages of fractionation of the Skaergaard intrusion, east Greenland. *Mineralogical Magazine*, 31, 511-543.
- Buddington, A.F., and Lindsley, D.H. (1964) Iron-titanium oxide minerals and synthetic equivalents. *Journal of Petrology*, 5, 310-357.
- Carmichael, I.S.E. (1967a) The mineralogy of Thingmuli, a Tertiary volcano in eastern Iceland. *American Mineralogist*, 52, 1815-1841.
- (1967b) The iron-titanium oxides of salic volcanic rocks and their associated ferromagnesian silicates. *Contributions to Mineralogy and Petrology*, 14, 36-64.
- (1991) The redox states of basic and silicic magmas: A reflection of their source regions. *Contributions to Mineralogy and Petrology*, 106, 129-141.
- Carmichael, I.S.E., Turner, F.J., and Verhoogen, J. (1974) *Igneous petrology*, 739 p. McGraw-Hill, New York.
- Czamanske, G.K., and Mihalik, P. (1972) Oxidation during magmatic differentiation, Finnmarka Complex, Oslo area, Norway: Part I, The opaque oxides. *Journal of Petrology*, 13, 493-509.
- Czamanske, G.K., and Wones, D.R. (1973) Oxidation during magmatic differentiation, Finnmarka Complex, Oslo area, Norway: Part 2, The mafic silicates. *Journal of Petrology*, 14, 349-380.
- Druitt, T.H., and Bacon, C.R. (1989) Petrology of the zoned calcalkaline magma chamber of Mount Mazama, Crater Lake, Oregon. *Contributions to Mineralogy and Petrology*, 101, 245-259.
- Dymek, R.F., and Gromet, L.P. (1984) Nature and origin of orthopyroxene megacrysts from the St. Urbain Anorthosite Massif, Quebec. *Canadian Mineralogist*, 22, 297-326.
- Emslie, R.F. (1980) Geology and petrology of the Harp Lake Complex, central Labrador: An example of Elsonian magmatism. *Geological Survey of Canada, Bulletin* 293, 136 p.
- Ewart, A., Green, J.C., Carmichael, I.S.E., and Brown, F.H. (1971) Volcanic low-temperature rhyolitic magmas in New Zealand. *Contributions to Mineralogy and Petrology*, 33, 128-144.
- Ewart, A., Hildreth, W., and Carmichael, I.S.E. (1975) Quaternary acid magmas in New Zealand. *Contributions to Mineralogy and Petrology*, 51, 1-27.
- Frost, B.R., and Lindsley, D.H. (1991) Occurrence of iron-titanium oxides in igneous rocks. In *Mineralogical Society of America Reviews in Mineralogy*, 25, 433-468.
- Frost, B.R., Lindsley, D.H., and Andersen, D.J. (1988) Fe-Ti oxide-silicate equilibria: Assemblages with fayalitic olivine. *American Mineralogist*, 73, 727-740.
- Frost, B.R., Fyfe, W.S., Tazake, K., and Chan, T. (1989) Grain-boundary graphite in rocks and implications for high electrical conductivity in the lower crust. *Nature*, 340, 134-136.
- Frost, B.R., Frost, C.D., Lindsley, D.H., Scoates, J.S., and Mitchell, J.N. (1992) The Laramie Anorthosite Complex and the Sherman Batholith: Geology, evolution, and theories for origin. In A.W. Snoke and J.R. Steidtmann, Eds., *Geology of Wyoming*, in press. Geological Survey of Wyoming, Laramie, Wyoming.
- Fuhrman, M.L., Frost, B.R., and Lindsley, D.H. (1988) Crystallization conditions of the Sybille Monzonite, Laramie Anorthosite Complex, Wyoming. *Journal of Petrology*, 29, 699-729.
- Ghiorso, M.S., and Sack, R.O. (1991) Fe-Ti oxide geothermometry: Thermodynamic formulation and the estimation of intensive variables in silicic magmas. *Contributions to Mineralogy and Petrology*, 108, 485-510.
- Hildreth, W. (1977) The magma chamber of the Bishop Tuff: Gradients in pressure, temperature, and composition. Ph.D. dissertation, University of California, Berkeley, California.
- (1979) The Bishop Tuff: Evidence for the origin of compositional zonation in silicic magma chambers. *Geological Society of America Special Paper*, 180, 45-75.
- (1983) The compositionally zoned eruption of 1912 in the Valley of Ten Thousand Smokes, Katmai National Park, Alaska. *Journal of Volcanology and Geothermal Research*, 18, 1-56.
- Himmelberg, G.R., and Ford, A.B. (1976) Pyroxenes of the Dufek Intrusion. *Journal of Petrology*, 17, 219-243.
- (1977) Iron-titanium oxides of the Dufek Intrusion, Antarctica. *American Mineralogist*, 62, 623-633.
- Howie, R.A. (1955) The geochemistry of the charnockite series of Madras, India. *Transactions of the Royal Society of Edinburgh*, 62, 725-768.
- Janardhan, A.S., Newton, R.C., and Hansen, E.C. (1982) The transformation of amphibolite facies gneiss to charnockite in southern Karnataka and northern Tamil Nadu, India. *Contributions to Mineralogy and Petrology*, 79, 130-149.
- Johnson, R.W., and Arculus, R.J. (1978) Volcanic rocks of the Witu Islands, Papua New Guinea: The origin of magmas above the deepest part of the New Britain Benioff Zone. *Bulletin of Volcanology*, 41, 609-655.
- Lindsley, D.H., and Frost, B.R. (1992) Equilibria among Fe-Ti oxides, pyroxenes, olivine, and quartz: Part I. Theory. *American Mineralogist*, 77, 987-1003.
- Lindsley, D.H., Brown, G.M., and Muir, I.D. (1969) Conditions of the ferrowollastonite-ferrohedenbergite inversion in the Skaergaard Intrusion, East Greenland. *Mineralogical Society of America Special Paper* 2, 193-201.
- Lindsley, D.H., Frost, B.R., Andersen, D.J., and Davidson, P.M. (1990) Fe-Ti oxide-silicate equilibria: Assemblages with orthopyroxene. In R.J. Spencer and I.-M. Chou, Eds., *Fluid-mineral interactions: A Tribute to H.P. Eugster*, special publication 2, p. 103-119. The Geochemical Society, San Antonio, Texas.
- Lindsley, D.H., Frost, B.R., Ghiorso, M.S., and Sack, R.O. (1991) Oxides lie: The Bishop Tuff did not erupt from a thermally zoned magma body. *Eos*, 72, 312.

- Lu, F., and Anderson, A.T. (1991) Mixing origins of volatile and thermal gradients in Bishop magma. *Eos*, 72, 312.
- Malm, O.A., and Ormaasen, D.E. (1978) Mangarite-charnockite intrusives in the Lofoten-Vesterålen area, North Norway: Petrography, chemistry and petrology. *Norges Geologiske Undersøkelse Bulletin*, 338, 83–114.
- Mathison, C.I. (1967) The Somerset Dam layered basic intrusion, southeastern Queensland. *Journal of the Geological Society of Australia*, 14, 57–86.
- (1975) Magnetite and ilmenite in the Somerset Dam layered basic intrusion, southeastern Queensland. *Lithos*, 8, 93–111.
- Mathison, C.I., and Hamlyn, P.R. (1987) The McIntosh layered troctolite-olivine gabbro intrusion, East Kimberley, Western Australia. *Journal of Petrology*, 28, 211–234.
- Molyneux, T.C. (1972) X-ray data and chemical analyses of some titanomagnetite and ilmenite samples from the Bushveld Complex, South Africa. *Mineralogical Magazine*, 38, 863–871.
- Morse, S.A. (1979) Kiglapait geochemistry. II. Petrography. *Journal of Petrology*, 20, 394–410.
- (1980) Kiglapait mineralogy. II. Fe-Ti oxide minerals and the activities of oxygen and silica. *Journal of Petrology*, 21, 685–719.
- Morse, S.A., Lindsley, D.H., and Williams, R.J. (1980) Concerning intensive parameters in the Skaergaard Intrusion. *American Journal of Science*, 280A, 159–170.
- Naldrett, A.J., Bray, J.G., Gasparrini, E.L., Podolsky, T., and Rucklidge, J.C. (1970) Cryptic variation and the petrology of the Sudbury nickel irruptive. *Economic Geology*, 65, 122–155.
- Naslund, H.R. (1980) Part I, Petrology of the Upper Border Group of the Skaergaard Intrusion East Greenland; and Part II, An experimental study of liquid immiscibility in iron-bearing silicate melts. Ph.D. dissertation, University of Oregon, Eugene, Oregon.
- (1984) Petrology of the upper border series of the Skaergaard Intrusion. *Journal of Petrology*, 23, 185–212.
- Osborn, E.F. (1959) Role of oxygen pressure in the crystallization and differentiation of basaltic magma. *American Journal of Science*, 257, 609–647.
- Parsons, I. (1981) The Klokken Gabbro-Syenite Complex, South Greenland: Quantitative interpretation of mineral chemistry. *Journal of Petrology*, 22, 233–260.
- Patchen, A.D. (1987) Petrology and stratigraphy of the Lake Owen layered mafic complex, S.E. Wyoming. M.S. thesis, University of Wyoming, Laramie, Wyoming.
- Percival, J.A. (1992) Orthopyroxene-poikilitic tonalites of the Desliens igneous suite, Ashuanipi granulite complex, Labrador–Quebec, Canada. *Canadian Journal of Earth Science*, 28, 743–753.
- Ravindra Kumar, G.R., Srikantappa, C., and Hansen, E. (1985) Charnockite formation at Ponmudi in southern India. *Nature*, 313, 207–209.
- Roeder, P.L., and Campbell, I.H. (1985) The effect of postcumulus re-
actions on composition of chrome-spinels from the Jimberlana intrusion. *Journal of Petrology*, 26, 763–786.
- Rutherford, M.J. (1984) Melatroctolite-anorthositic gabbro complex, Cumberland, Rhode Island: Petrology, origin, and regional setting. *Geological Society of America Bulletin*, 95, 844–854.
- Sato, M., and Valenza, M. (1980) Oxygen fugacities of the layered series of the Skaergaard intrusion, East Greenland. *American Journal of Science*, 280A, 134–158.
- Singer, B.S., Myers, J.D., and Frost, C.D. (1992) Mid-Pleistocene lavas from the Seguam volcanic center, central Aleutian arc: Closed-system fractional crystallization of a basalt to rhyodacite eruptive suite. *Contributions to Mineralogy and Petrology*, 110, 87–112.
- Snoke, A.W., Quick, J.E., and Bowman, H.R. (1981) Bear Mountain igneous complex, Klamath Mountains, California: an ultrabasic to silicic calc-alkalic suite. *Journal of Petrology*, 22, 501–552.
- Taylor, H.P., and Forester, R.W. (1979) An oxygen and hydrogen isotope study of the Skaergaard intrusion and its country rocks: A description of a 55-m.y.-old fossil hydrothermal system. *Journal of Petrology*, 20, 355–419.
- Thy, P. (1982) Titanomagnetite and ilmenite in the Fongen-Hyllingen Complex, Norway. *Lithos*, 15, 1–16.
- Vincent, E.A., and Phillips, R. (1954) Iron-titanium oxide minerals in layered gabbros of the Skaergaard Intrusion, East Greenland. *Geochimica et Cosmochimica Acta*, 6, 1–26.
- Wager, L.R., and Brown, G.M. (1968) Layered igneous rocks. W.H. Freeman, San Francisco.
- Weiss, S. (1986) Petrogenese des intrusivkomplexes von Ballachulish, Westschottland: Kristallisationsverlauf in einem zonierten Kaledonischen Pluton. Ph.D. dissertation, University of Munich, Munich, Germany.
- Weiss, S., and Troll, G. (1989) The Ballachulish Igneous Complex, Scotland: Petrography, mineral chemistry, and order of crystallization in the monzodiorite-quartz diorite suite and in the granite. *Journal of Petrology*, 30, 1069–1115.
- Willemsse, J. (1969) The vanadiferous magnetic iron ore of the Bushveld Complex. *Economic Geology Monograph* 4, 187–208.
- Williams, R.J. (1971) Reaction constants in the system Fe-MgO-SiO₂-O₂: Intensive parameters in the Skaergaard intrusion, East Greenland. *American Journal of Science*, 271, 132–146.
- Wilson, J.R., Ebensen, K.H., and Thy, P. (1981) Igneous petrology of the synorogenic Fongen-Hyllingen layered basic complex, south-central Scandinavian Caledonides. *Journal of Petrology*, 22, 584–627.
- Wright, T.L., Kinoshita, W.T., and Peck, D.L. (1968) March 1965 eruption of Kilauea Volcano and the formation of Makaopuhi Lava Lake. *Journal of Geophysical Research*, 73, 3181–3205.

MANUSCRIPT RECEIVED FEBRUARY 12, 1991

MANUSCRIPT ACCEPTED MAY 4, 1992